NASA TM X-697

TECHNICAL MEMORANDUM

X-697

ANALYTICAL INVESTIGATION OF THE REENTRY BEHAVIOR OF THE "FLYING WIND TUNNEL" TEST VEHICLE, WITH SOME EFFECTS OF THRESHOLD AND TORQUE LEVEL OF A ROLL-RATE CONTROL SYSTEM

By Byron M. Jaquet and Herman S. Fletcher

Langley Research Center
Langley Station, Hampton, Va.

NATIONAL AERONAUTICS AND SPACE ADMINISTRATION
WASHINGTON
July 1962

NATIONAL AERONAUTICS AND SPACE ADMINISTRATION

TECHNICAL MEMORANDUM X-697

ANALYTICAL INVESTIGATION OF THE REENTRY BEHAVIOR OF THE "FLYING WIND TUNNEL" TEST VEHICLE, WITH SOME EFFECTS OF THRESHOLD AND TORQUE LEVEL OF A ROLL-RATE CONTROL SYSTEM*

By Byron M. Jaquet and Herman S. Fletcher

SUMMARY

An analytical investigation was made in order to determine the effects of various initial conditions on the dynamic behavior during reentry of the "flying wind tunnel" test vehicle. It was found that, when the atmosphere is reentered at an altitude of 400,000 feet with an initial angle of attack of 10°, the character of the angle-of-attack time history was affected to only a small degree by model support pylon misalinement and initial roll rate. At an altitude of 160,000 feet (where the model package would be jettisoned so that the central body with recorded data could be recovered), the frequency of the angle-of-attack oscillation was 1 cycle per second and the amplitude was about 1.3°. Of the initial conditions investigated, it was found that the roll rate of the vehicle was the most sensitive to pylon misalinement. For two opposing pylons differentially misalined about $1\frac{1}{2}^\circ$ a rapid buildup in roll rate occurred as the vehicle descended so that at an altitude of 160,000 feet the rate was about 23° per second which would be considered excessive. Also, the roll rate and roll angle were found to vary approximately linearly with changes in pylon misalinement at a given time.

With two opposing pylons differentially misalined about $1\frac{1}{2}^\circ$, the most critical of the initial conditions, a roll-rate control system with a torque of 250 foot-pounds operating outside of a threshold of 4° per second was the most effective of the arrangements studied in reducing the roll rate. At an altitude of 160,000 feet, for example, this control arrangement reduced the roll rate to about 6° per second from about 23° per second for the control-off case. There was a corresponding reduction in roll angle from about 71° to 34°.

*Title, Unclassified.

For a reentry with an initial angle of attack of 0° and no configurational asymmetries the amplitudes of the angle-of-attack oscillation would be about one-tenth of that for a reentry with an initial angle of attack of 10°.

INTRODUCTION

The flight conditions associated with reentry from lunar missions or hypersonic gliding flight (high Mach number at high altitude) cannot be presently duplicated in ground facilities. Also, experiments with rocket-propelled test vehicles have not been made in this flight regime. Thus, some degree of uncertainty exists in the aerodynamic, heating, and structural knowledge concerning this flight regime. In order to bridge the gap between information available from ground facilities and that information required for the design of vehicles operating at high altitudes and high Mach numbers, a flight experiment referred to as the "flying wind tunnel" has been proposed. In this program six instrumented models would be mounted on stings and pylons from a central body. In order to provide symmetry about the central body center line, the models would be mounted in diametrically opposed pairs and the plane of symmetry of each pair displaced 60° circumferentially. In each pair of models one model would be used to measure heating and pressure data and the other would be used to obtain static force data. The three pairs of models would be mounted at angles of attack of 0°, 15°, and 50° with respect to the central body. The test vehicle would be rocket boosted on a ballistic trajectory to such speeds and altitudes that, upon reentering the atmosphere, data would be obtained over a Mach number range of about 23 to 19 as the vehicle descended from an altitude of 400,000 feet to 160,000 feet. An automatic attitude control system would orient the vehicle to within ±3° of the velocity vector. At an altitude of about 160,000 feet the models would probably begin to fail structurally because of the high thermal conditions and therefore the model package would be jettisoned so that recorded data in the central body could be recovered. For this program to be successful, one of the prime requisites is that the vehicle possess a degree of stability sufficient to prevent the occurrence of large erratic motions.

Accordingly, a brief analytical investigation has been made, using the equations of motion of reference 1, to determine the effect of various initial conditions on the dynamic behavior of the vehicle during reentry from an altitude of 400,000 feet. Included in the investigation were the effects of initial angle of attack (angles of 0°, 3°, and 10° were investigated, the emphasis being on an angle of attack of 10°), relative lateral displacement between the center of gravity and the center of pressure (referred to hereinafter as center-of-gravity offset), initial roll rate, model support pylon misalinement, and aerodynamic damping derivatives.

The effectiveness of an on-off jet-reaction roll-rate control system in reducing the roll rate induced by model support pylon misalinement was also investigated. In this phase of the investigation, control system threshold and torque level were varied.

All calculations were made on an IBM 7090 electronic data processing system for a spherical nonrotating earth with the 1956 ARDC atmosphere.

SYMBOLS

The symbols and coefficients used herein are referred to the axes system of figure 1.

A reference area, sq ft

a_V total deceleration, $\frac{-\Delta V}{g\,\Delta t}$, g units

a speed of sound, ft/sec

C_X coefficient of force along X_b-axis, $\frac{\text{Force along } X_b\text{-axis}}{QA}$

C_Y coefficient of force along Y-axis, $\frac{\text{Force along Y-axis}}{QA}$

C_{Y_α} rate of change of side-force coefficient with angle of attack in XY-plane, $\frac{\partial C_Y}{\partial \alpha_Y}$, per radian

C_{Y_β} rate of change of side-force coefficient with angle of sideslip in XY-plane, $\frac{\partial C_Y}{\partial \beta}$, per radian

C_Z coefficient of force along Z-axis, $\frac{\text{Force along Z-axis}}{QA}$

C_{Z_α} rate of change of normal-force coefficient with angle of attack in XZ-plane, $\frac{\partial C_Z}{\partial \alpha_Z}$, per radian

C_m pitching-moment coefficient, $\frac{\text{Moment about Y-axis}}{QAd}$

[redacted]

C_{m_q} damping-in-pitch parameter, $\frac{\partial C_m}{\partial \frac{qd}{2V}}$

C_{m_α} variation of pitching-moment coefficient with angle of attack in XZ-plane, $\frac{\partial C_m}{\partial \alpha_Z}$, per radian

C_n yawing-moment coefficient, $\frac{\text{Moment about Z-axis}}{QAd}$

C_{n_r} damping-in-yaw parameter, $\frac{\partial C_n}{\partial \frac{rd}{2V}}$

C_{n_α} variation of yawing-moment coefficient with angle of attack in XY-plane, $\frac{\partial C_n}{\partial \alpha_Y}$, per radian

C_l rolling-moment coefficient, $\frac{\text{Moment about } X_b\text{-axis}}{QAd}$

C_l' rolling-moment coefficient due to differentially misalined model support pylons

C_{l_p} damping-in-roll parameter, $\frac{\partial C_l}{\partial \frac{pd}{2V}}$

d reference diameter, ft

f frequency of angle-of-attack oscillation, cycles/sec

g acceleration of gravity at earth's surface, 32.2 ft/sec^2

h altitude above earth's surface, ft

$I_{X,b}$ moment of inertia about X_b-axis, slug-ft^2

$I_{Y,b}$ moment of inertia about Y_b- and Z_b-axes, slug-ft^2

K roll-rate control threshold, deg/sec or radians/sec

M Mach number, V/a

[redacted]

M_X torque applied by roll-rate control about X_b-axis, ft-lb

m mass of vehicle, slugs

p,q,r angular rate about X-, Y-, and Z-axis, respectively, radians/sec or deg/sec

p_b, q_b, r_b angular rate about X_b-, Y_b-, and Z_b-axis, respectively, radians/sec or deg/sec

Q dynamic pressure, $\frac{\rho V^2}{2}$, lb/sq ft

R_e radius of earth, 20.925738×10^6 ft

t time, sec

u,v,w components of velocity along X-, Y-, and Z-axis, respectively, ft/sec

V resultant velocity, $\sqrt{u^2 + v^2 + w^2}$, ft/sec

X,Y,Z ballistic axes with origin at vehicle center of gravity; plane containing Z-axis is always parallel to X'Z'-plane (see fig. 1)

X_b, Y_b, Z_b body system of axes with origin at vehicle center of gravity and rolling through an angle ϕ about X-axis which is coincident with X_b-axis

X',Y',Z' reference axes with origin at vehicle center of gravity at some distance from center of earth and parallel to earth-fixed X_i, Y_i, and Z_i axes

α total angle of attack, angle between vehicle longitudinal axis and resultant velocity, $\sin \alpha = \frac{\sqrt{v^2 + w^2}}{V}$, deg or radians

α_Y angle of attack in XY-plane, $\tan^{-1} \frac{v}{u}$, deg or radians

α_Z angle of attack in XZ-plane, $\tan^{-1} \frac{w}{u}$, deg or radians

θ angle of elevation of X- and X_b-axes above a plane parallel to $X_i Z_i$-plane, radians

ϕ roll angle about X- and X_b-axes measured from Y-axis, radians or deg

ψ angle in X'Z'-plane between plane containing X- and Y-axes and X'-axis, radians or deg

ρ density of air (1956 ARDC standard tables), slugs/cu ft

Δ increment

Subscript:

o initial conditions

SCOPE OF INVESTIGATION

Reentry Conditions

All calculations were made from initial reentry conditions (see table I) at an altitude of 400,000 feet with a flight-path angle of -21.67° and a resultant velocity of 21,200 feet per second. The calculations made to determine the effects of various initial conditions on vehicle behavior are summarized in table II.

A combination of $\phi_o = 0^{\circ}$ with a center-of-gravity offset results in an initial trim angle in the lateral direction (along Y-axis of fig. 1) whereas a combination of $\phi_o = 90^{\circ}$ with a center-of-gravity offset results in an initial trim angle in the vertical direction (along Z-axis of fig. 1). The value of C_l' of 0.003 corresponds to a differential deflection between two opposing model support pylons of about $1\frac{1}{2}^{\circ}$. Ideally, the vehicle would reenter with $\alpha_o = p_o = \phi_o = C_l'$ = Center-of-gravity offset = 0. However, because of manufacturing tolerances, equipment placement, and gyro drift errors of the attitude control system, the vehicle would experience initial conditions at reentry other than zero but well within the range of values covered in table II. (The angle of attack at reentry is anticipated to be less than 3°.)

The roll-rate control system used was of the on-off type and operated without lag outside of a given threshold value, the control torque being applied to reduce or attempt to reduce the roll rate to within the threshold value.

All calculations were made on an IBM 7090 electronic data processing system using the equations of motion of reference 1 for a spherical

nonrotating earth and the 1956 ARDC atmosphere. It was necessary to modify the rolling-moment equation of reference 1 to include $C_{l_p} \frac{pd}{2V}$, and $C_{l'}$ terms.

Mass, Dimensional, and Aerodynamic Parameters

The various mass, dimensional, and aerodynamic parameters are given in table I for the vehicle which is shown in figure 2. The aerodynamic parameters were considered to be constant for the Mach number range covered in the investigation (≈23 to 18).

The values of the parameters C_X, C_{Y_α}, C_{Z_α}, C_{m_α}, and C_{n_α} were obtained from the Langley Flight Reentry Programs Office and were estimated by using an empirical modification of experimental values obtained for a configuration similar to that shown in figure 2 and accounting for differences in central body shape, model support pylon, and Mach number.

The damping parameters were estimated by determining the individual central body, pylon, and model parameters about their respective centers of gravity and then transferring, with appropriate nondimensionalization, to the vehicle center of gravity. Newtonian values (ref. 2) were used for the central body and the pylon values were estimated by considering equivalent rectangular wedges. The effectiveness of the wedge on the pylon parameters was determined from reference 3. Model wing-alone parameters were determined from references 4 and 5. In addition, certain necessary parameters of the models at angles of attack of 0°, 15°, and 50° such as lift, drag, pitching-moment, and static sideslip data were available from unpublished wind-tunnel tests at a Mach number of 22. The effect of the central body and the pylons on C_{l_p} was determined from reference 6 with the value of C_{l_p} for the equivalent rectangular wing obtained from reference 4. Where possible, the contribution of the vertical tails of the models to the damping derivatives was estimated from the static derivatives of the tail determined from unpublished wind tunnel data. For example,

$$\left(C_{l_p}\right)_{tail} = 2\left(C_{Y_\beta}\right)_{tail}\left(\frac{\text{Vertical distance between model center of gravity and tail center of pressure}}{\text{Model reference length}}\right)^2$$

where $\left(C_{Y_\beta}\right)_{tail}$ is the rate of change of the lateral force of the

tail with sideslip angle and was experimentally determined at the appropriate angle of attack. Mutual interference between models, pylons, and the central body was not considered in the estimation of the damping derivatives.

RESULTS AND DISCUSSION

Trajectory Characteristics

Inasmuch as the trajectories considered herein were for the most part in the altitude region where the dynamic pressure was low, there was essentially no effect of the various initial conditions investigated on the variation with time of such trajectory parameters as M, V, a_V, Q, and h. Therefore, in order to relate the dynamic behavior to the trajectory parameters, figures 3 and 4 are presented as being representative for the cases investigated.

Dynamic Behavior With Control System Inoperative

As previously noted, the equations of motion for the present investigation were those of reference 1. In the discussion of the dynamic behavior of the vehicle in terms of the total angle of attack (which is the angle between the total velocity vector and the longitudinal axis of the vehicle and is defined as $\sin^{-1}\left(\frac{\sqrt{v^2 + w^2}}{V}\right)$, it was found desirable to discuss the translational velocities v and w in the axes system for which the equations of motion were written. This presentation was necessary in order to describe effectively the planes in which the angular motions take place because the body-axes angles of attack α_Y and α_Z were not an output of the computational program. Body-axes angular rates, however, were computed. The axes system (fig. 1) differs from the usual body-axes system in that the Z-axis is constrained to remain in a plane parallel to the X_i, Z_i inertial plane and in that the body is free to spin about the X_b axis which is coincident with the X-axis. The X-axis is always alined with the axis of symmetry of the body. The equations used in reference 1 are in a form frequently used in ballistics work and hereinafter the X,Y,Z-axes system will be referred to as the ballistic-axes system in order to differentiate between it and the body-axes system.

Time histories of the total angle of attack α, body-axes roll rate p_b, body-axes pitch rate q_b, body-axes yaw rate r_b, and in some

cases roll angle ϕ have been used to determine the effects of various initial conditions on the dynamic behavior of the vehicle and are presented in figures 5 to 10. In figure 11, the frequency of the angle-of-attack oscillation is presented as a function of altitude for a typical six-degree-of-freedom calculation and a one-degree-of-freedom approximation. Also, representative translational velocities along the ballistic Y- and Z-axes are presented for several calculations in figure 12.

Since a reentry with an initial angle of attack of 10° would impose more severe behavior requirements than for probable reentries at angles of attack of 0° or 3°, most of the discussion is concerned with this condition. The data are presented for an altitude range between 400,000 and 130,000 feet but the discussion is concerned primarily with altitudes down to 160,000 feet.

Reentry at $\alpha_o = 10^\circ$.- If the vehicle were to enter the atmosphere with an initial angle of attack of 10° in the ballistic plane (fig. 5(a)) without configurational asymmetries, the angle-of-attack motion is seen to be an oscillation, about a trim angle of attack of 0°, of decreasing amplitude and increasing frequency. The initial buildup in the angle of attack, in the high altitude range, is associated with a downward curving flight path while the vehicle attitude remains unchanged since an aerodynamic restoring moment is essentially nonexistent because of the extremely low air density. At an altitude of 160,000 feet the amplitude of the angle of attack has decreased to about 1.3° and the frequency of oscillation at this point is about 1 cycle per second. A typical plot of frequency against altitude is shown in figure 11 and is representative of the various cases investigated. For comparison purposes the one-degree-of-freedom approximation of the frequency is also shown in figure 11. No rolling or yawing (fig. 5(b)) is associated with the reentry at $\alpha_o = 10^\circ$ without configurational asymmetries and the maximum pitch rate (fig. 5(c)) at an altitude of 160,000 feet is about 10° per second whereas for a reentry at $\alpha_o = 0^\circ$ the pitch rate is about 1° per second as will be shown later.

A 4.9-percent-diameter center-of-gravity offset introduced in the lateral plane $(\phi_o = 0^\circ)$ results in a total angle of attack which is a combination of an angle of attack in the ballistic XZ-plane and an effective sideslip angle in the ballistic XY-plane. Therefore, as the vehicle descends, the total angle of attack has certain minimum values (short-dashed curve, fig. 5(a)) which, for these initial conditions, correspond closely to the trim sideslip angle at the particular time. An indication of the angles of attack and sideslip in the ballistic axes system are illustrated by the translational velocities in figure 12 for several cases including those in which the total angle of attack is presented in figure 5(a). In figure 12 are presented time histories

of v and w, the translational velocities along the ballistic Y- and Z-axes, respectively. Therein it can be seen that for the case of $\phi_o = 0^o$ and a 4.9-percent-diameter center-of-gravity offset the velocity w, indicative of an angle of attack, becomes zero at $t \approx 14.3$ seconds and v, which is indicative of a sideslip angle, has a value which corresponds approximately to the minimum total angle of attack at this time as shown in figure 5(a). Further, as the vehicle descends it oscillates (fig. 12) about $w = 0$, corresponding to zero angle of attack and some value of v corresponding to a sideslip angle with the result that the total angle of attack $\sin^{-1}\left(\frac{\sqrt{v^2 + w^2}}{V}\right)$ never reaches zero (fig. 5(a)). The center-of-gravity offset in the lateral plane $(\phi_o = 0^o)$ causes a small amount of yawing and rolling about the body axes and causes the vehicle to trim at a roll angle of about 1.9° (fig. 5(b)) but does not affect the pitch rate (fig. 5(c)).

In the case of the center-of-gravity offset initially in the vertical plane $(\phi_o = 90^o)$ the vehicle trims about a positive angle of attack (fig. 6(a)) and there is no sideslip involved. This condition is also indicated by the translational velocities v and w in the ballistic axes system in figure 12. As the vehicle descends, the total angle of attack (fig. 6(a)) decreases at a rate about the same as that with no center-of-gravity offset so that at an altitude of 160,000 feet the amplitude is about 2.1°. When the center of gravity is offset initially in the vertical direction, the Y_b-axis which contains the center of pressure and the center of gravity now is in the vertical plane (see axes system, fig. 1) and consequently there is no tendency to roll (figs. 6(b) and 6(c)), there is no pitching about the body axes (fig. 6(d)), and the yaw rate (fig. 6(e)) increases in a manner similar to the pitch rate when the center of gravity is offset in the lateral direction (fig. 6(d)).

In order to determine the sensitivity of the roll rate and roll angle to changes in pylon misalinement, two values of C_l' were investigated with a 4.9-percent-diameter center-of-gravity offset initially at $\phi_o = 0^o$. Values of C_l' of 0.003 and 0.001 are representative of two opposing pylons differentially misalined about $1\frac{1}{2}^o$ and $1/2^o$, respectively. Each of the values investigated caused only small changes in the total angle of attack (fig. 7(a)), the largest change occurring at an altitude of about 160,000 feet. This change in angle of attack results from the rapid buildup in roll rate (fig. 7(b)) with decreasing altitude. The roll rate (fig. 7(b)) and roll angle (fig. 7(c)) at a given time vary in an essentially linear manner with changes in pylon misalinement. For example, at an altitude of 160,000 feet roll rates

of about 8.6° and 22.5° per second and roll angles of about 24° and 72° are associated with values of C_l' of 0.001 and 0.003, respectively.

Since the primary purpose of the flying wind tunnel is to obtain accurate data in a region of low density air, it would appear to be desirable to keep the roll rate low in order to avoid possible cross-coupling effects and the resultant additional complexity in data reduction. Thus, it would appear that, unless the model support pylons are almost exactly alined, there is a need for a roll-rate control system. The body-axes pitch and yaw rates (figs. 7(d) and 7(e)) vary considerably as the vehicle descends and differ appreciably for the two values of C_l' because of the difference in the buildup of the roll rate. In neither case, however, do the pitch and yaw rates exceed 10° per second for the altitude range of interest.

Although it has been shown that the rolling associated with pylon misalinement could be detrimental, it is of interest to determine the effect of a small initial roll rate on the motions. A comparison $(C_l' = 0)$ of the data of figures 6(a) and 8(a) indicates that, if the vehicle was initially oriented with the center-of-gravity offset at $\phi_o = 0°$, an initial roll rate of 10° per second would slightly reduce peak angles of attack for altitudes below about 250,000 feet whereas the converse is true when the center-of-gravity offset is in the vertical direction $(\phi_o = 90°)$. The pitch and yaw rates (figs. 8(d) and 8(e)) for the vehicle with $p_o = 10°$ per second do not exceed 10° per second for the altitude range of interest.

When the vehicle with an initial roll rate of 10° per second has pylon misalinement superimposed upon it, there is only a small change in angle of attack (fig. 8(a)) and the increase in roll rate (fig. 8(b)) builds up with decreasing altitude in a manner similar to that for the vehicle with $p_o = 0°$ per second (fig. 6(b)). The pitch and yaw rates (figs. 8(d) and 8(e)) are modified considerably but are less than 10° per second.

In order to determine the influence of the damping derivatives on the motions, a computation was made for the vehicle initially rolling at 10° per second with the damping derivatives zero about all three axes. The results of this calculation are shown in figure 9 along with the results for a previous calculation in which the damping derivatives had the values shown in table I. All results in figure 9 are for a 4.9-percent-diameter center-of-gravity offset initially in the lateral direction $(\phi_o = 0°)$ and are without pylon misalinement. The dynamic behavior of the vehicle is only slightly affected by a lack of aerodynamic damping, the effect being noticeable (fig. 9) only in the altitude range below about 200,000 feet which is where the dynamic pressure (fig. 3) begins to increase rapidly. Allen's stability factor (ref. 7),

in terms of the coefficients used herein, is $-2C_X + C_{Z_\alpha} + C_{m_{qd/2V}} \frac{d^2m}{2I_{Y,b}}$, neutral stability being indicated by a value of zero. Because of the large stable value of C_{Z_α} (-5.905) the vehicle could have a value of C_{m_q} of 6.39 and still possess neutral stability. Thus, it would be expected that a change in C_{m_q} from -9.393 to 0 would have only a minor effect on the motions as was previously noted.

L 2 0 5 8

Reentry at $\alpha_o = 0^\circ$.- Should it be possible to achieve an ideal reentry ($\alpha_o = 0^\circ$ and no configurational asymmetries) the angle of attack of the vehicle would be reduced by about a factor of 10 as compared with a reentry at $\alpha_o = 10^\circ$ (fig. 5(a)). This effect would hold for the entire altitude range investigated and, in addition, as was the case of the reentry at $\alpha_o = 10^\circ$, there would be no rolling or yawing (fig. 5(b)) and the pitch rate (fig. 5(c)) would also be reduced by a factor of about 10 so that at an altitude of 160,000 feet the vehicle reentering with $\alpha_o = 0^\circ$ would be pitching at a rate of 1° per second.

Introducing pylon misalinement ($C_l' = 0.003$) had no noticeable effect on the angle of attack (see fig. 10(a)) and, as was the case for a reentry at $\alpha_o = 10^\circ$, caused a rapid buildup in the roll rate (fig. 10(b)) and roll angle (fig. 10(c)) as the vehicle descended into the more dense air. Also, the pylon misalinement caused only small changes in the pitch and yaw rates (figs. 10(d) and 10(e)).

A 4.9-percent-diameter center-of-gravity offset in the lateral ($\phi_o = 0^\circ$) or vertical ($\phi_o = 90^\circ$) direction along with pylon misalinement caused the vehicle to trim at an angle of attack of about 0.9° for most of the trajectory. (See fig. 10(a).) The frequency of the angle-of-attack oscillation for reentries at $\alpha_o = 0^\circ$ was essentially the same as for reentries at $\alpha_o = 10^\circ$. The center-of-gravity offset had only a small effect on the roll rate (fig. 10(b)) and the pitch and yaw rates (figs. 10(c) and 10(d)) are less than 2° per second for altitudes down to 130,000 feet.

Effectiveness of Roll-Rate Control System

As previously noted, it would be desirable to maintain a low roll rate; however, if the model support pylons were misalined, a rapid buildup in the roll rate would occur as the vehicle descends. In order to determine the effectiveness of a roll-rate reaction control system

in reducing the large roll rates associated with pylon misalinement calculations were made for a control system which would become operative at threshold values of 2° or 4° per second with a torque level of 50 foot-pounds and 4° or 8° per second with a torque level of 250 foot-pounds. The purpose of these calculations was to determine control effectiveness for torque levels which would be representative of minimum or maximum available torque. All calculations were made with $C_l' = 0.003$ and a 4.9-percent center-of-gravity offset and, except for one case, with $\phi = 0^\circ$. Data on the control system operation are presented in figures 13 to 15. Note that on figures 13(b) and 14(b) intermittent operation indicates a region of rapid on-off operations.

L
2
0
5
8

Operation of the control system affects the angle of attack (fig. 13(a)) only for altitudes below about 200,000 feet where the angle of attack is reduced for all operating conditions investigated. The greatest reduction in angle of attack (fig. 13(a)) and roll rate (fig. 13(b)) occurs with a threshold of 4° per second and a torque of 250 foot-pounds; the reduction in angle of attack was small but at an altitude of 160,000 feet the roll rate was reduced by about 70 percent when compared with the control-system-off case. (See fig. 15.) With a torque level of 50 foot-pounds a system with a 2° per second threshold would operate initially at the highest altitude (fig. 13(b)) of the systems investigated but would reduce the roll rate by only about 40 percent at an altitude of 160,000 feet (fig. 15). For a 4° per second threshold, the 250 foot-pound system would operate for about one-half the time of the 50 foot-pound system but for the same nozzle locations the high torque case would require a total impulse of about $2\frac{3}{4}$ times that of the low torque level. The higher torque level would, of course, provide a much greater reduction in roll rate than the low torque level. As the roll rate is reduced by increasing the torque for a given threshold, the pitch and yaw rates (figs. 13(d) and 13(e)) tend toward values for $C_l' = 0$ case (figs. 5(b) and 5(c)) as would be expected.

The data of figure 14 illustrate that, when $\phi_o = 90^\circ$ where the rolling tendency is initially the least the control system is more effective since the buildup in roll rate is not as great as for the case of $\phi_o = 0^\circ$ (fig. 13(b)).

Supplemental Results for a Reentry With an Initial Angle of Attack of 3° With Control System in Operation

On the basis of the results just discussed and additional information on the vehicle system characteristics, a reentry with an initial angle of attack of 3° was considered more within the realm of the system

capabilities. Also, closer tolerances could be achieved in locating equipment so that the center-of-gravity offset would be 2 percent instead of 4.9 percent d. Therefore, a calculation was made for these conditions with a roll-rate control system operating with a torque level of 250 foot-pounds outside of a threshold of 5° per second. The results of this calculation are presented in figure 16 and are for $\phi_o = 90^\circ$, $C_l' = 0.003$, and $p_o = 0^\circ$ per second.

The data of figure 16 are similar in trend to those data for reentries at $\alpha = 10^\circ$ and 0°. For altitudes below 200,000 feet the amplitude of the angle of attack is less than 1° and at an altitude of 160,000 feet it is about 0.8°. The pitch and yaw rates are less than 3° per second for the entire altitude range investigated. (See fig. 16(a).) For these initial conditions the roll-rate control system is sufficiently powerful to maintain the roll rate at a constant value of about 5° per second for altitudes between about 200,000 feet and 150,000 feet (fig. 16(b)). Associated with the constant roll rate is a linear change in roll angle (fig. 16(c)). The translational velocities v and w (fig. 16(d)) have been included to indicate the overall characteristics of the angles of attack α_Y and α_Z.

CONCLUSIONS

An analytical investigation of the effects of various initial conditions at reentry on the dynamic behavior of the "flying wind tunnel" test vehicle has indicated the following conclusions:

1. For reentries with an initial angle of attack of 10° the character of the angle-of-attack time history was affected to only a small degree by pylon misalinement and initial roll rate. At an altitude of 160,000 feet (where the model package would be jettisoned so that the central body with recorded data could be recovered), the frequency of the angle-of-attack oscillation was 1 cycle per second and the amplitude was about 1.3°.

2. Of the initial conditions investigated, it was found that the vehicle roll rate was the most sensitive to simulated pylon misalinement. For two opposing pylons differentially misalined about $1\frac{1}{2}^\circ$, a rapid buildup in roll rate occurred as the vehicle descended so that, at an altitude of 160,000 feet, the roll rate was about 23° per second which might be excessive for the vehicle. Also, the roll rate and roll angle were found to vary approximately linearly with changes in pylon misalinement at a given time.

3. With two opposing pylons differentially misalined about $1\frac{1}{2}^{\circ}$, the most critical of the initial conditions a roll-rate control with a torque of 250 foot-pounds operating outside of a threshold of 4° per second was the most effective, of the control arrangements studied, in reducing the roll rate. At an altitude of 160,000 feet, for example, this control arrangment reduced the roll rate to about 6° per second from about 23° per second for the control-off case. There was a corresponding reduction in roll angle from about 71° to 34°.

4. For a reentry with an initial angle of attack of 0° and no configurational asymmetries the amplitudes of the angle-of-attack oscillation would be about one-tenth of that with an initial angle of attack of 10°.

Langley Research Center,
National Aeronautics and Space Administration,
Langley Station, Hampton, Va., May 4, 1962.

[redacted]

REFERENCES

1. Jaquet, Byron M.: Dynamic Stability and Dispersion of a Project Mercury Test Capsule Upon Entering the Atmosphere, With Effects of Roll Rate, Center-of-Gravity Displacement, and Threshold of a Rate-Reaction Control System. NASA TM X-350, 1961.

2. Fisher, Lewis R.: Equations and Charts for Determining the Hypersonic Stability Derivatives of Combinations of Cone Frustums Computed by Newtonian Impact Theory. NACA TN D-149, 1959.

3. McLellan, Charles H.: A Method for Increasing the Effectiveness of Stabilizing Surfaces at High Supersonic Mach Numbers. NACA RM L54F21, 1954.

4. Harmon, Sidney M., and Jeffreys, Isabella: Theoretical Lift and Damping in Roll of Thin Wings With Arbitrary Sweep and Taper at Supersonic Speeds - Supersonic Leading and Trailing Edges. NACA TN 2114, 1950.

5. Martin, John C., Margolis, Kenneth, and Jeffreys, Isabella: Calculation of the Lift and Pitching Moments Due to Angle of Attack and Steady Pitching Velocity at Supersonic Speeds for Thin Sweptback Tapered Wings With Streamwise Tips and Supersonic Leading and Trailing Edges. NACA TN 2699, 1952.

6. Nielsen, Jack: Missile Aerodynamics. McGraw-Hill Book Co., Inc., c.1960.

7. Allen, H. Julian: Motion of a Ballistic Missile Angularly Misalined With the Flight Path Upon Entering the Atmosphere and Its Effect on Aerodynamic Heating, Aerodynamic Loads, and Miss Distance. NACA TN 4048, 1957.

[redacted]

TABLE I.- INITIAL CONDITIONS, MASS, DIMENSIONAL, AERODYNAMIC, AND CONTROL SYSTEM PARAMETERS

Initial altitude, ft			400×10^3
Initial flight-path angle, deg			-21.67
Initial resultant velocity, V_o, fps			21,200
Initial pitch rate, q_o, radians/sec			0
Initial yaw rate, r_o, radians/sec			0
Initial roll rate, p_o, radians/sec			0 or 0.1745
Initial roll angle, ϕ_o, deg			0 or 90
Initial elevation angle, θ_o, deg			0
Initial angle of attack, α_o, deg	0	3	10
u_o, fps	21,200	21,170.96	20,877.76
v_o, fps	0	0	0
w_o, fps	0	-1,109.61	-3,682.44
ψ_o, deg	-21.67	-18.67	-11.67
m, slugs			182.2
$I_{Y,b}$, slug-ft^2			4,700.0
$I_{X,b}$, slug-ft^2			1,760.0
A, sq ft			21.912
d, ft			5.280
C_X			-1.224
C_{Y_α}, per radian			-5.905
C_{Z_α}, per radian			-5.905
C_{m_α}, per radian			-3.732
C_{n_α}, per radian			3.732
C_{m_q}, per radian			-9.393
C_{n_r}, per radian			-9.393
C_{l_p}, per radian			-2.167
Control system:			
Threshold, deg/sec	2	4	8
Torque about X_b-axis, ft-lb	50	50 or 250	250

TABLE II.- SUMMARY OF AERODYNAMIC AND CONTROL PARAMETERS INVESTIGATED

α_o, deg	Center-of-gravity offset, percent d	ϕ_o, deg	p_o, deg/sec	$C_{l'}$	C_{m_q} and C_{n_r}	C_{l_p}	$M_{X,b}$, ft-lb	K, deg/sec
0	0	0	0	0	-9.393	-2.167	0	∞
0	0	0	0	.003	-9.393	-2.167	0	∞
0	4.9	0	0	.003	-9.393	-2.167	0	∞
0	4.9	90	0	.003	-9.393	-2.167	0	∞
10	0	0	0	0	-9.393	-2.167	0	∞
10	4.9	90	0	0	-9.393	-2.167	0	∞
10	4.9	0	0	0	-9.393	-2.167	0	∞
10	4.9	0	0	.001	-9.393	-2.167	0	∞
10	4.9	0	0	.003	-9.393	-2.167	0	∞
10	4.9	90	0	.003	-9.393	-2.167	0	∞
10	4.9	0	10	0	-9.393	-2.167	0	∞
10	4.9	0	10	.003	-9.393	-2.167	0	∞
10	4.9	90	10	0	-9.393	-2.167	0	∞
10	4.9	0	10	0	0	0	0	∞
10	4.9	90	0	0.003	-9.393	-2.167	50	2
10	4.9	0	0	.003	-9.393	-2.167	50	2
10	4.9	0	0	.003	-9.393	-2.167	50	4
10	4.9	0	0	.003	-9.393	-2.167	250	4
10	4.9	0	0	.003	-9.393	-2.167	250	8
*3	2.0	90	0	0.003	-9.393	-2.167	250	5

*Supplemental calculation made for conditions which are more representative of the tolerances of the vehicle and its systems.

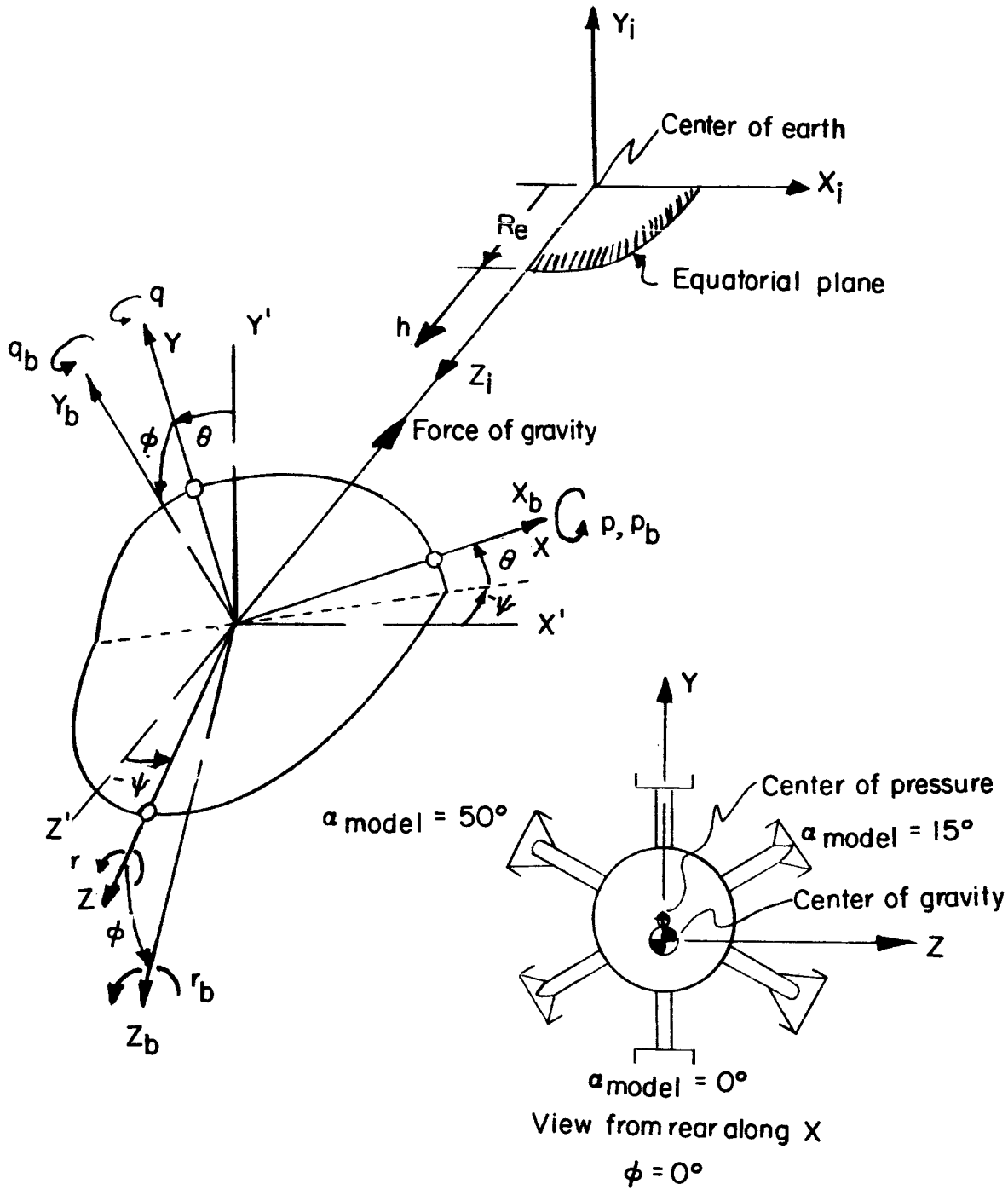

Figure 1.- Axes system.

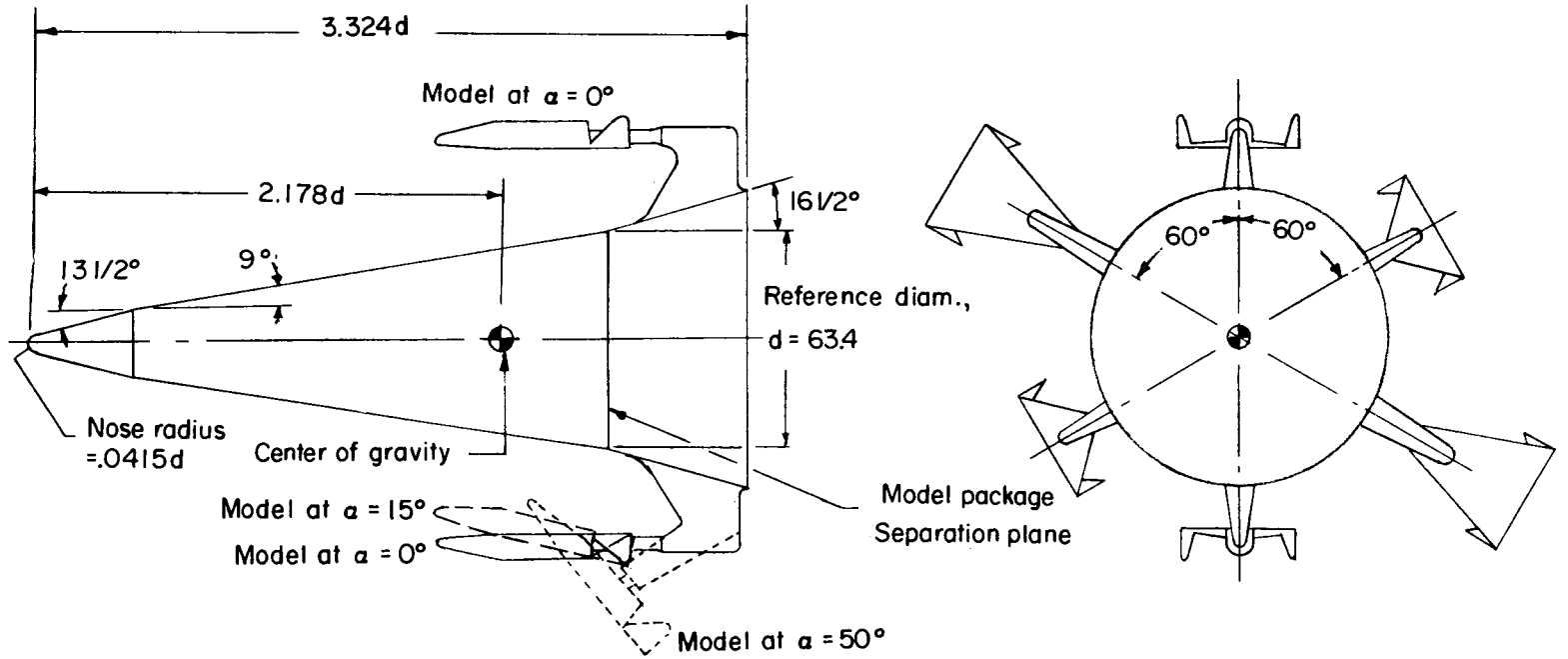

Figure 2.- General arrangement of test vehicle.

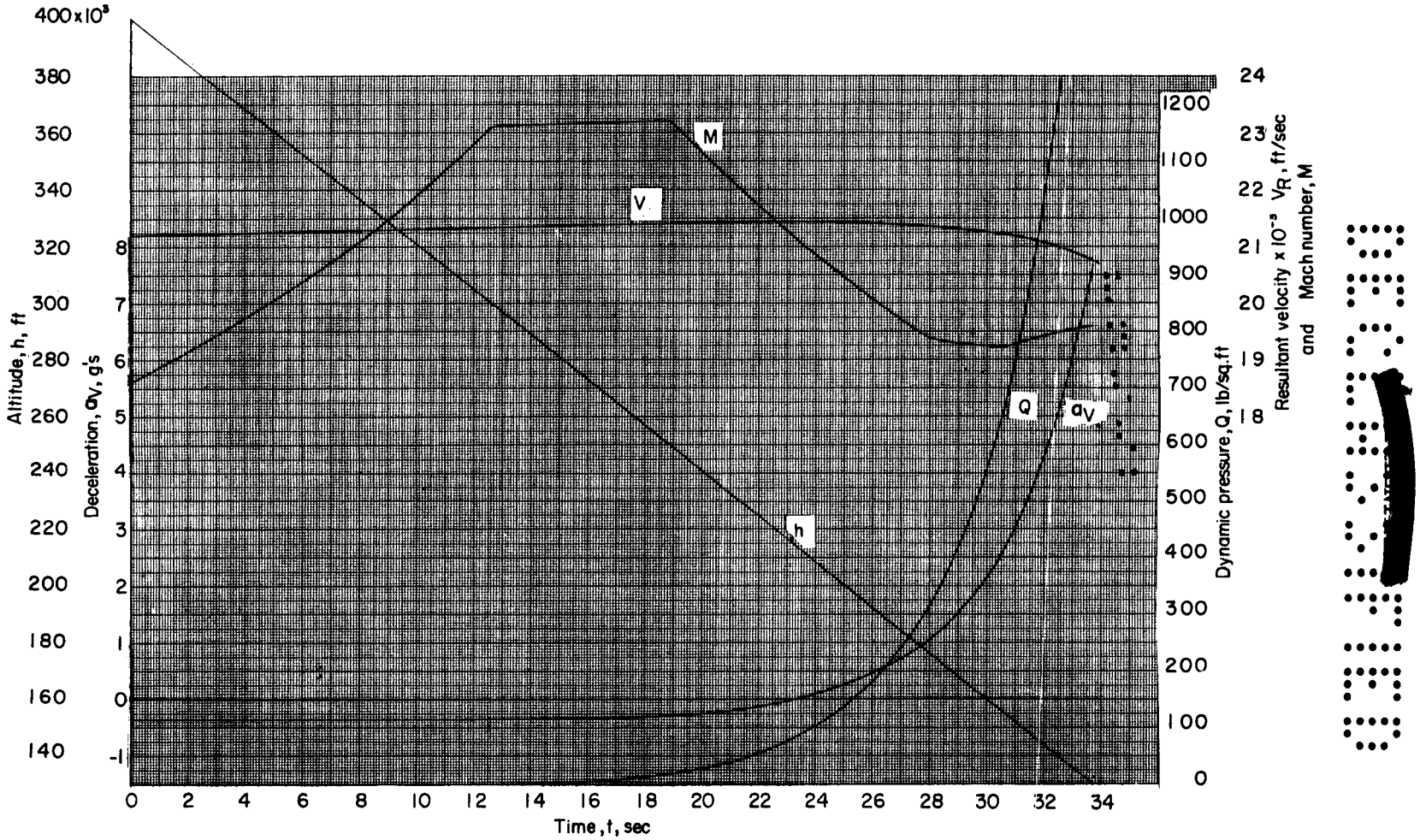

Figure 3.- Representative trajectory parameters.

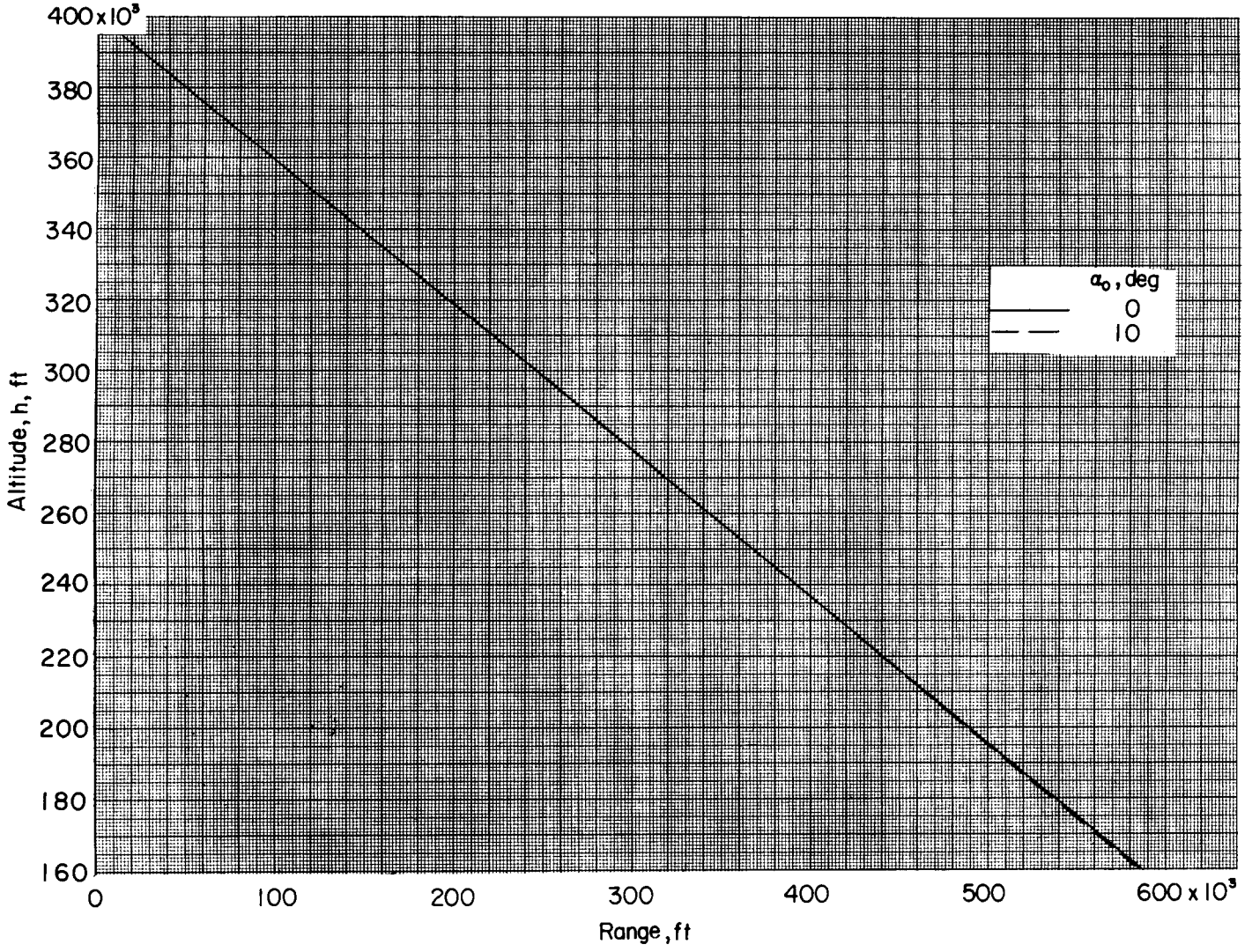

Figure 4.- Representative altitude—ballistic-range relationship.

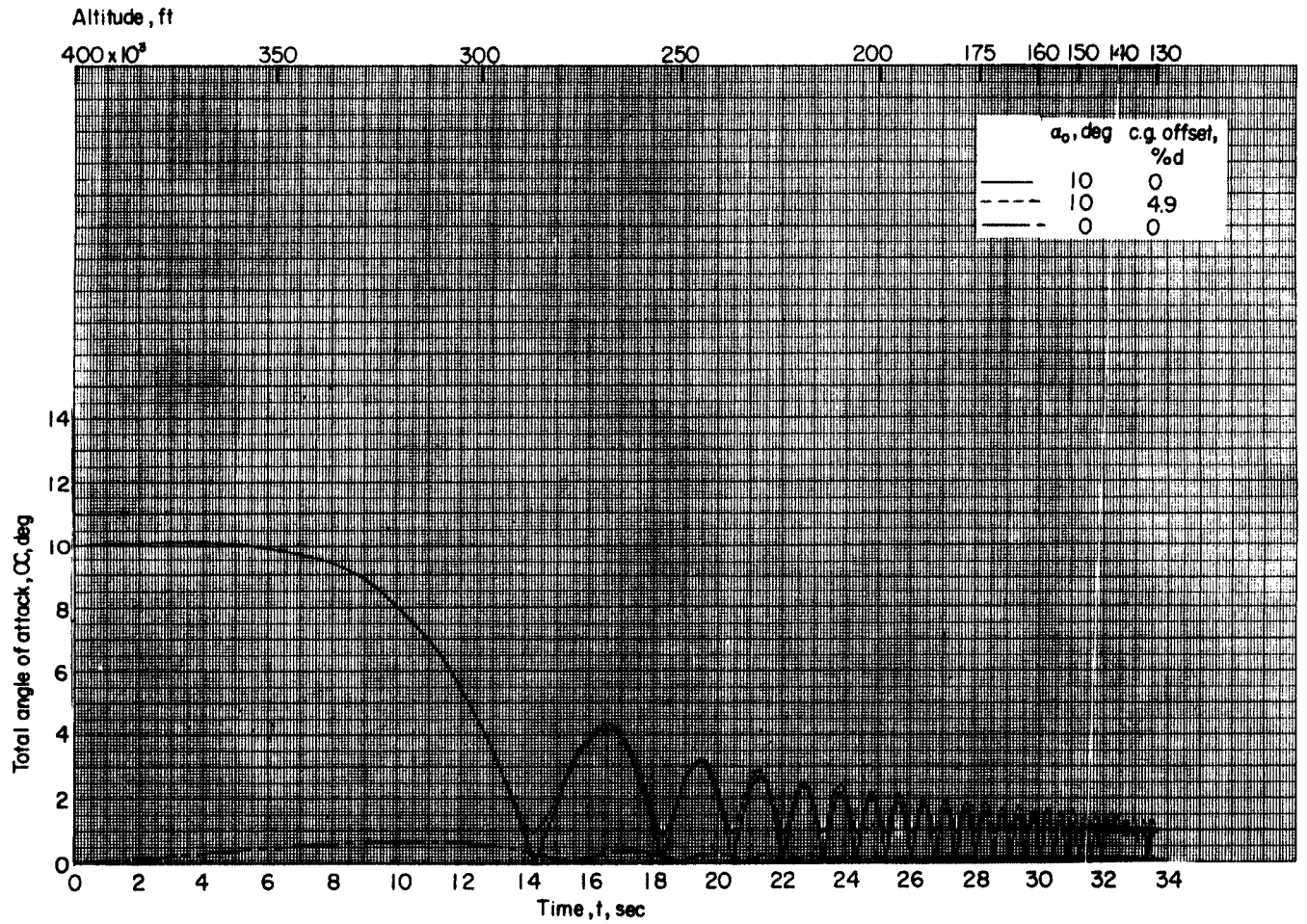

(a) Angle-of-attack time history.

Figure 5.- Effect of initial angle of attack and center-of-gravity offset on time histories. $p_o = 0^\circ$ per second; $\phi_o = 0^\circ$; $C_l' = 0$.

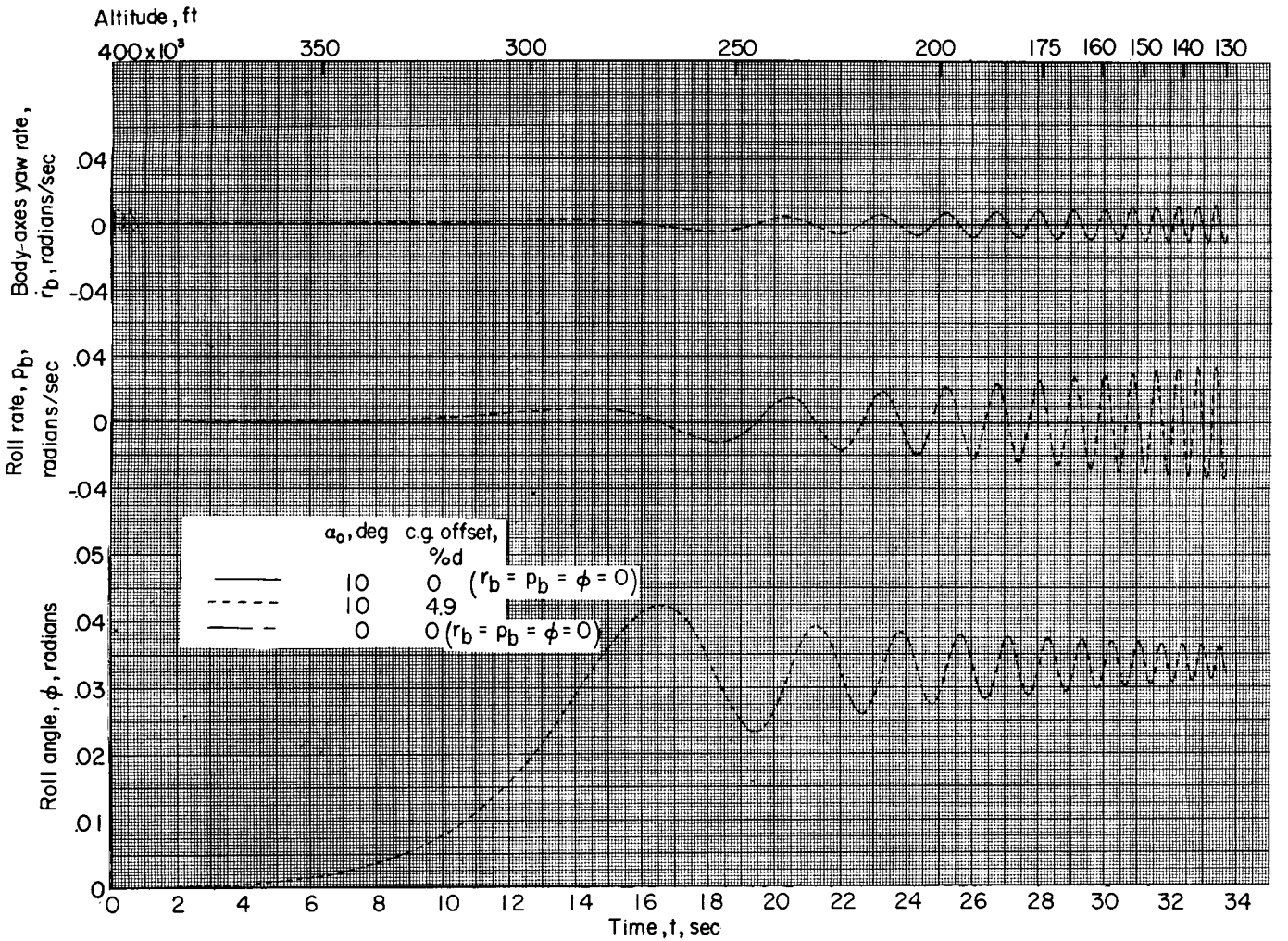

(b) Time histories of body-axes yaw rate, roll rate, and roll angle.

Figure 5.- Continued.

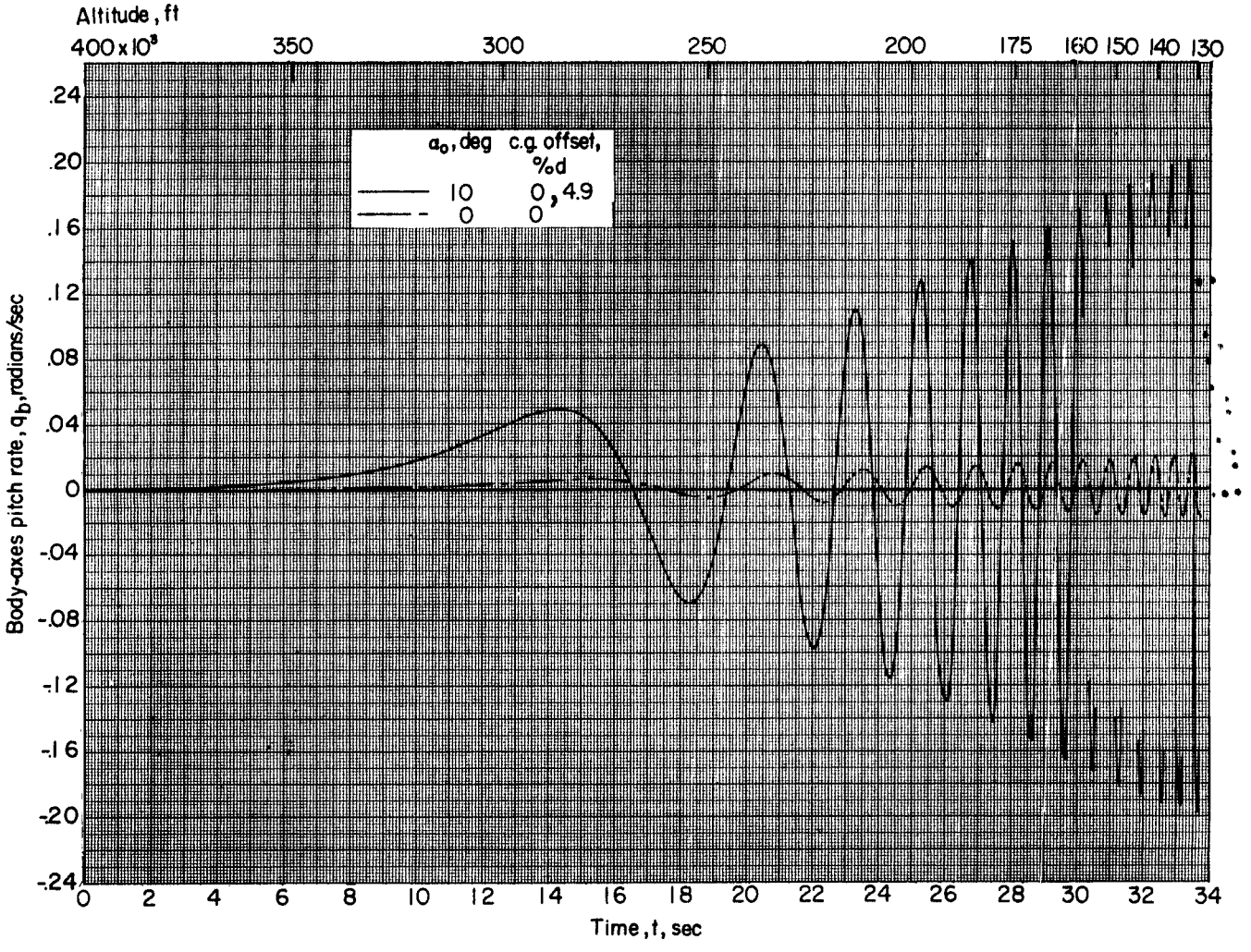

(c) Body-axes pitch-rate time history.

Figure 5.- Concluded.

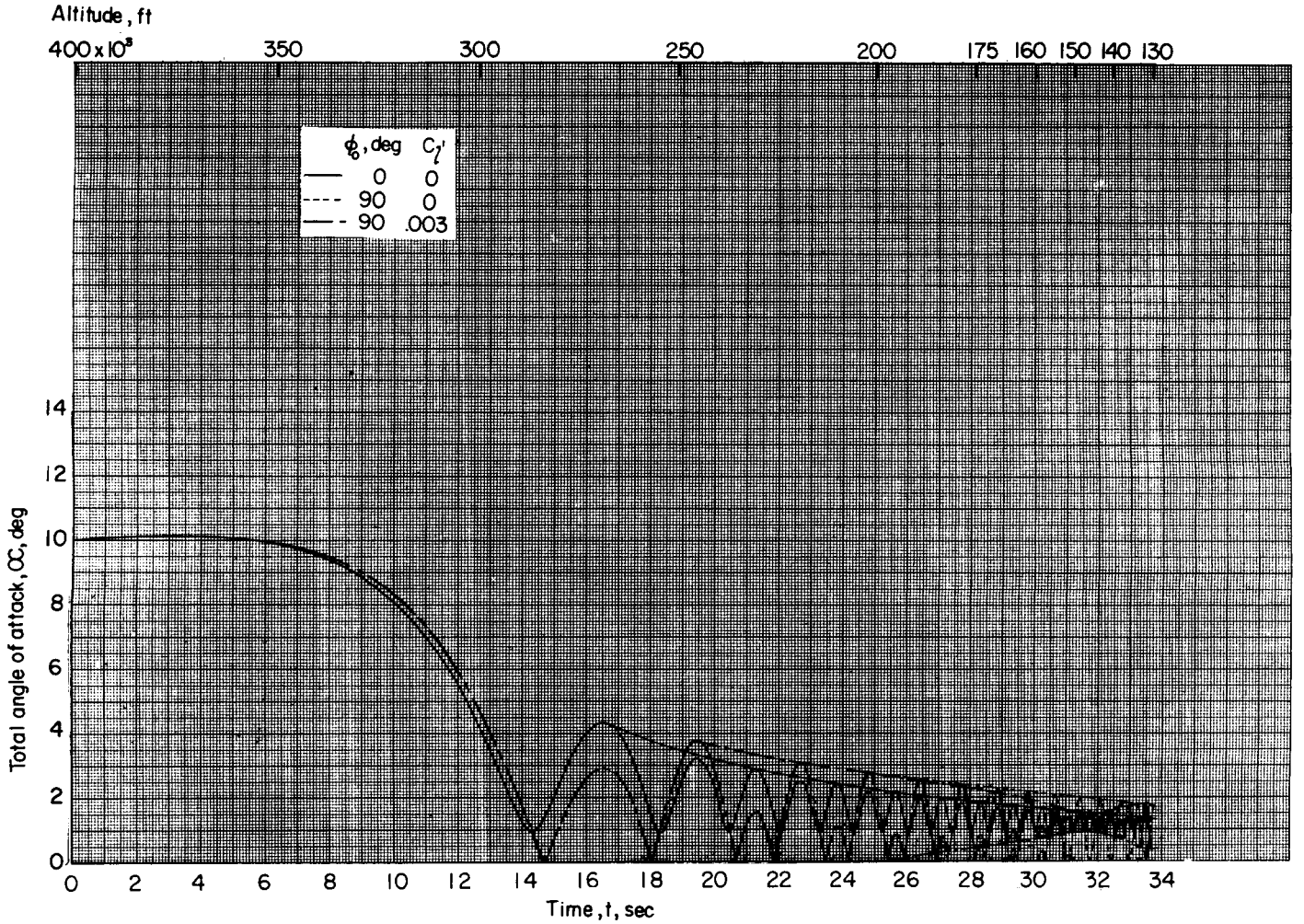

(a) Angle-of-attack time history.

Figure 6.- Effect of initial roll angle and pylon misalinement on time histories. $\alpha_o = 10^o$; $p_o = 0^o$ per second; center-of-gravity offset, 4.9 percent d.

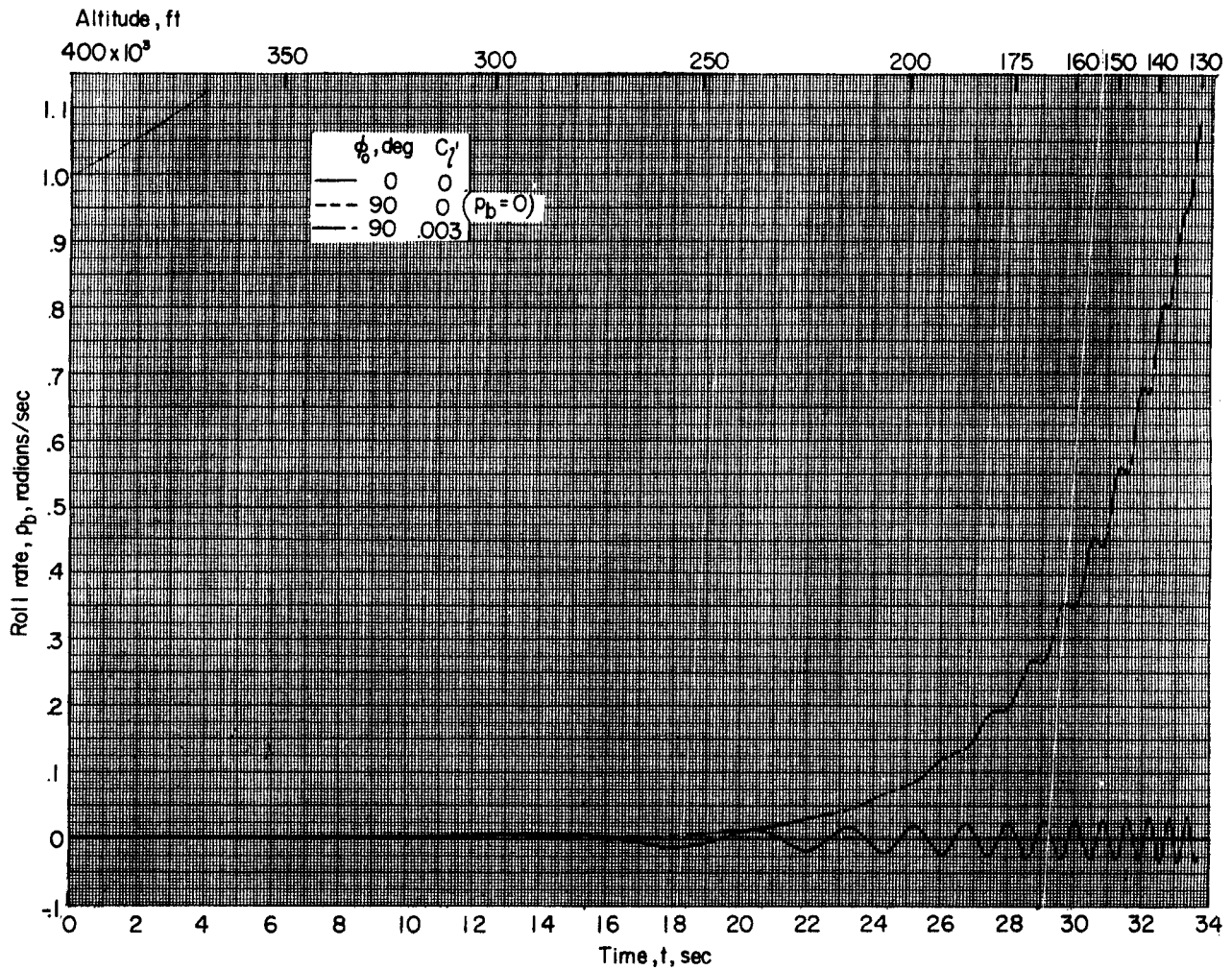

(b) Roll-rate time history.

Figure 6.- Continued.

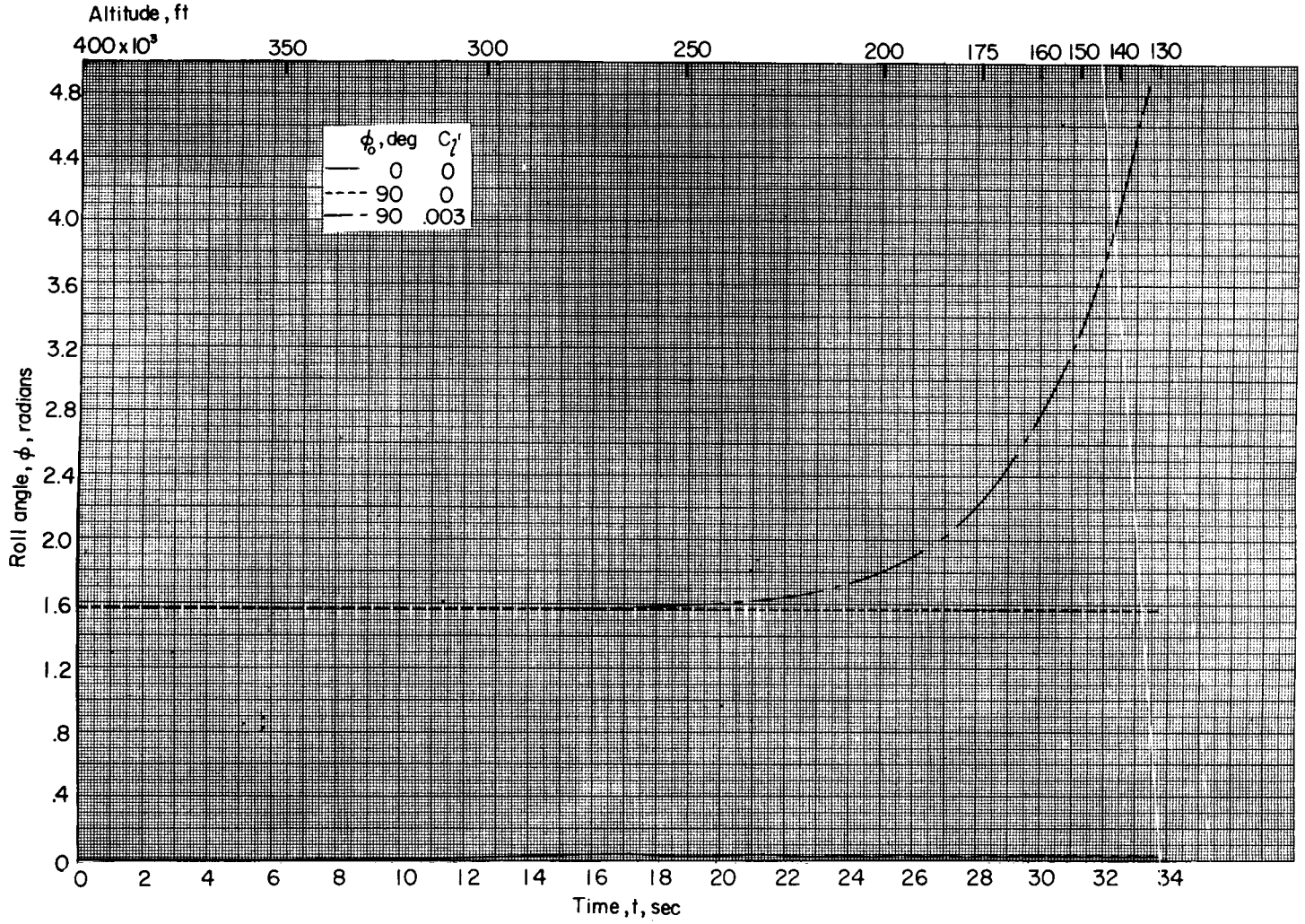

(c) Roll-angle time history.

Figure 6.- Continued.

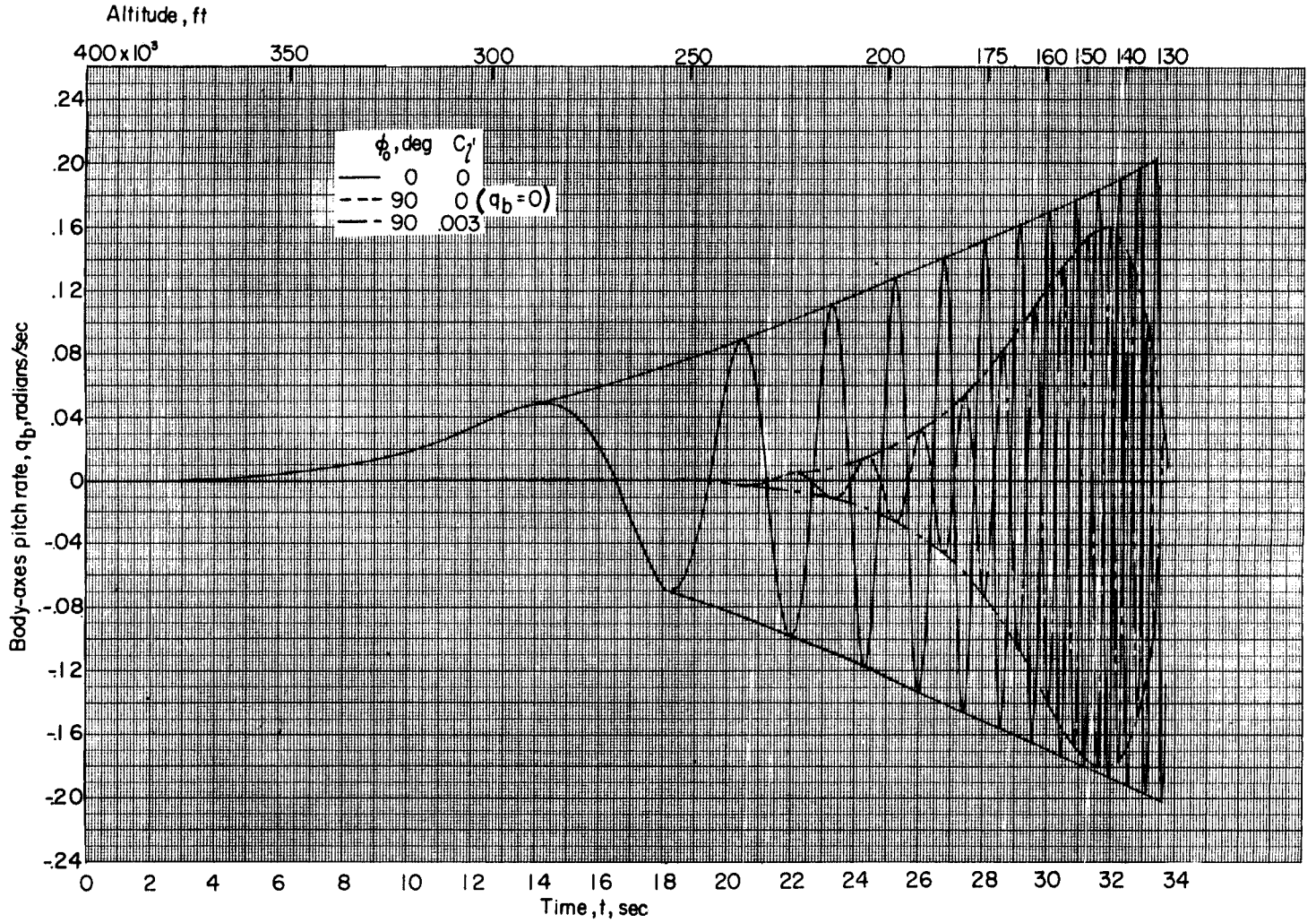

(d) Body-axes pitch-rate time history.

Figure 6.- Continued.

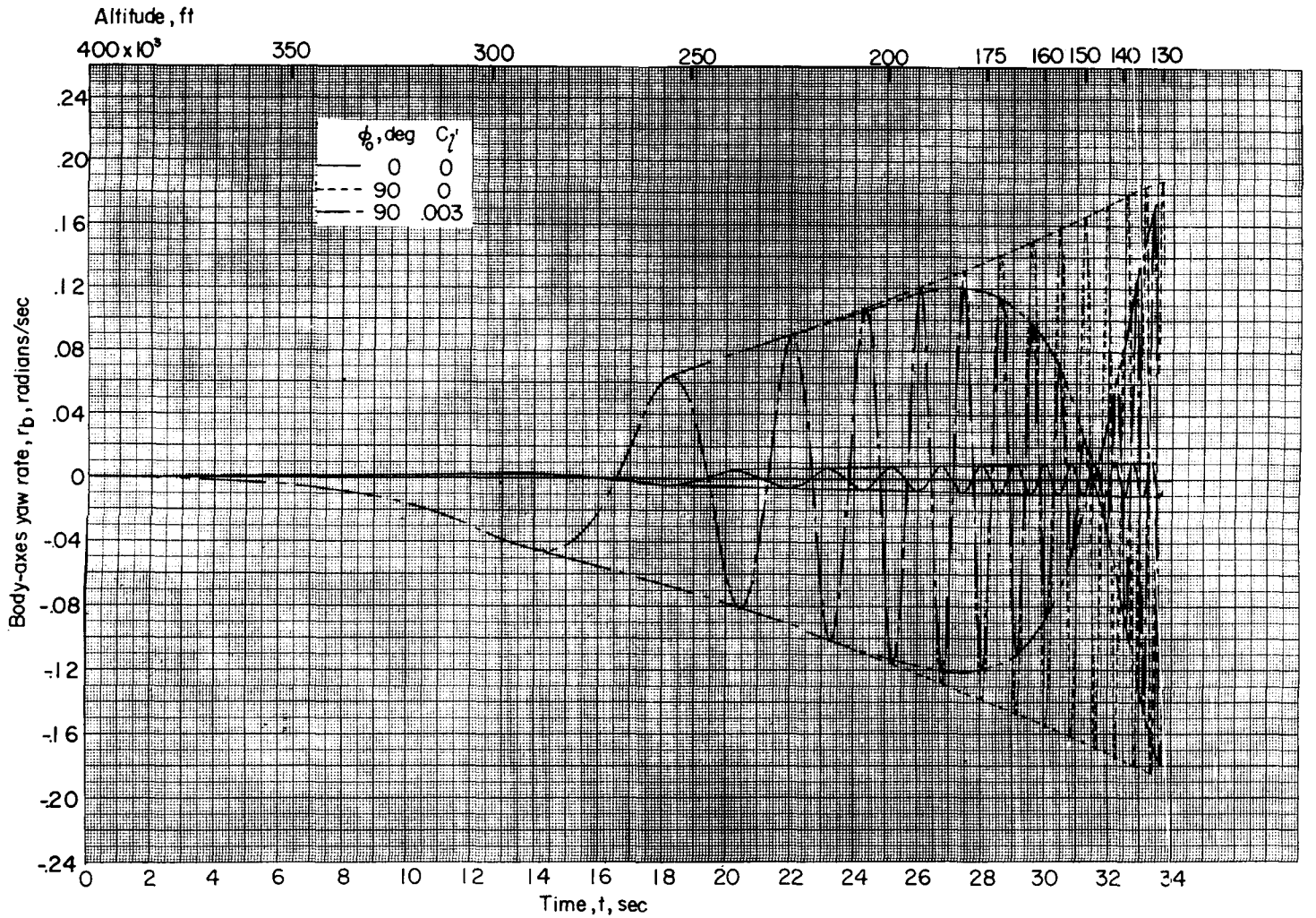

(e) Body-axes yaw-rate time history.

Figure 6.- Concluded.

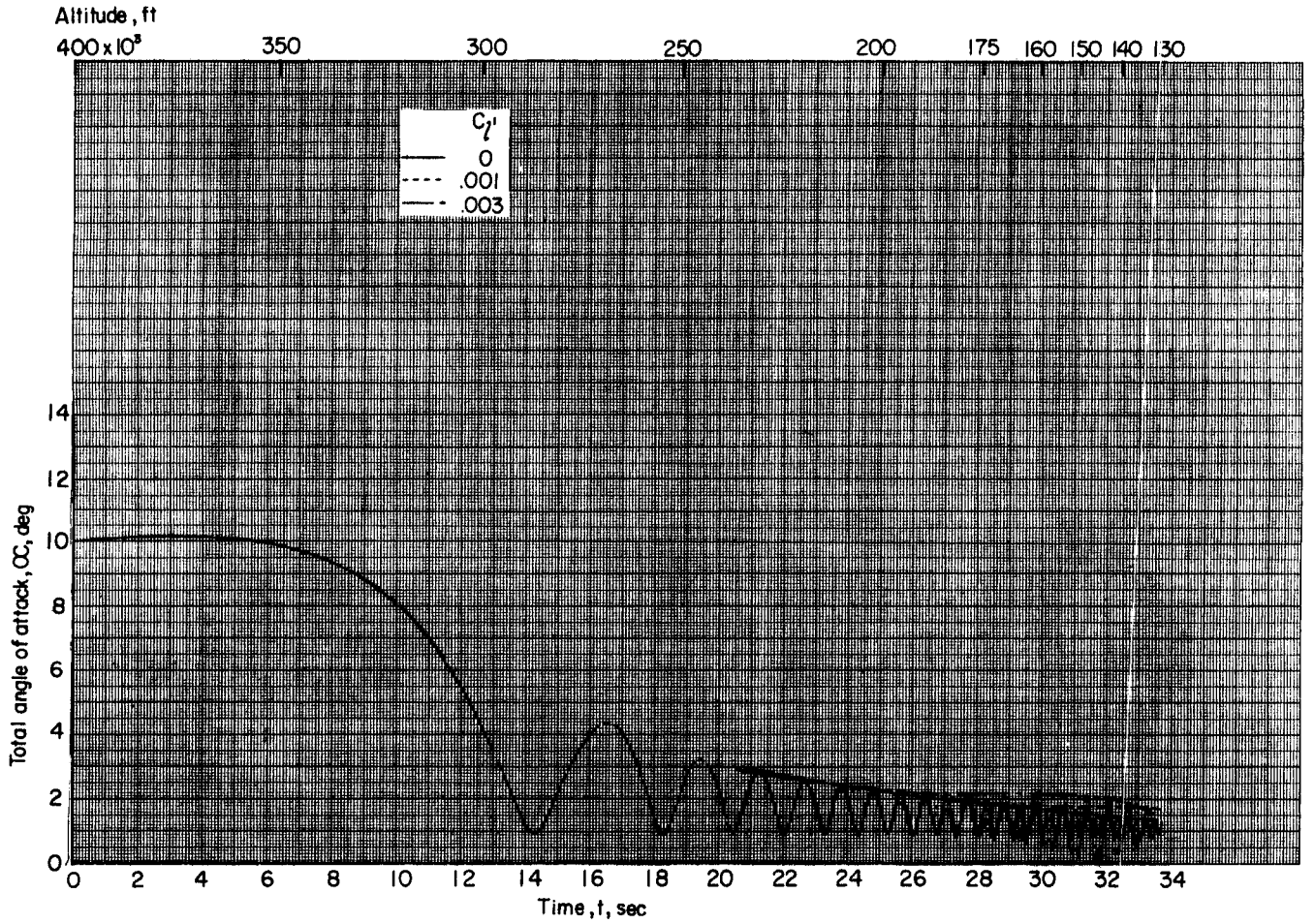

(a) Angle-of-attack time history.

Figure 7.- Effect of pylon misalinement on time histories. $\alpha_o = 10^o$; $p_o = 0^o$ per second; $\phi_o = 0^o$; center-of-gravity offset, 4.9 percent d.

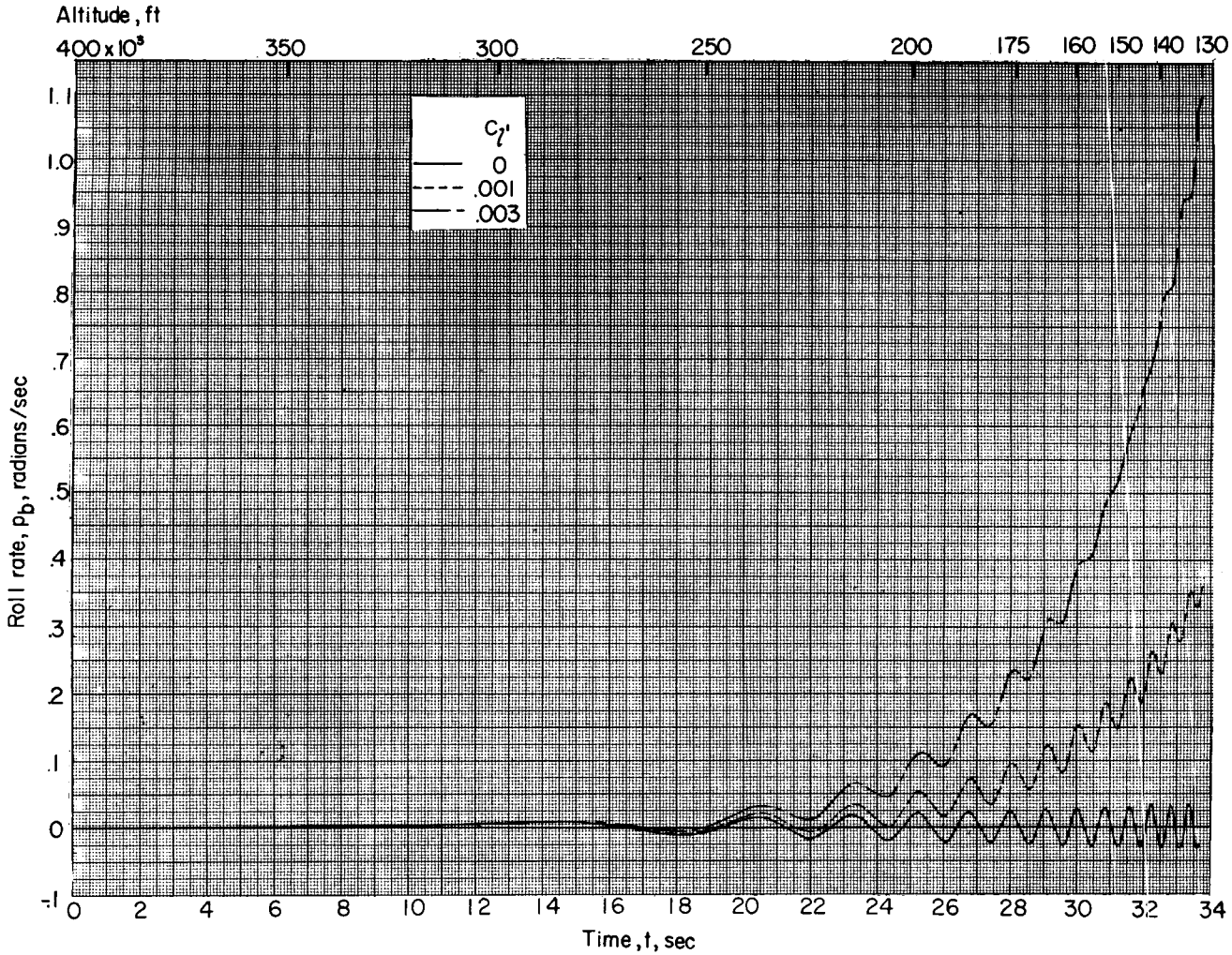

(b) Roll-rate time history.

Figure 7.- Continued.

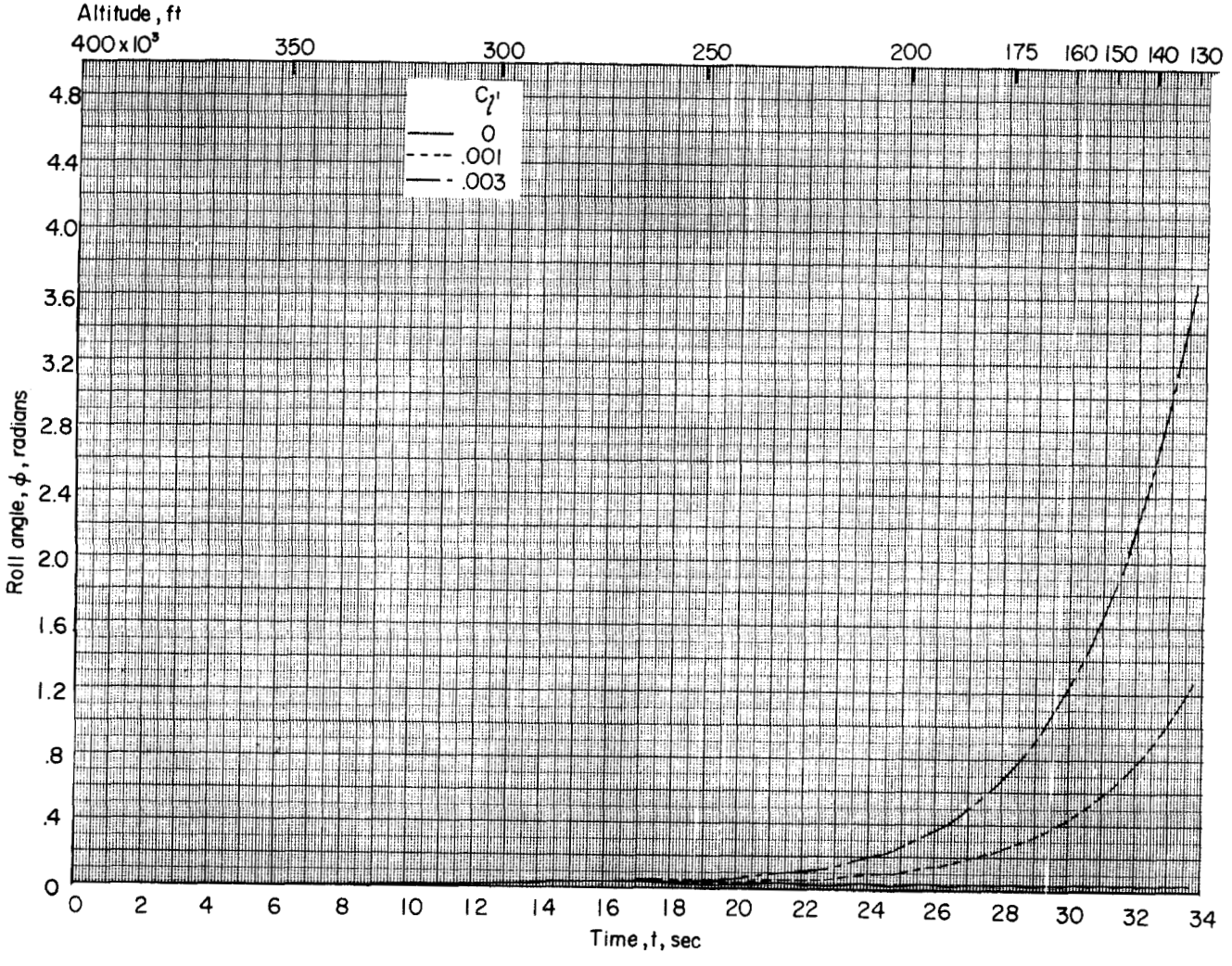

(c) Roll-angle time history.

Figure 7.- Continued.

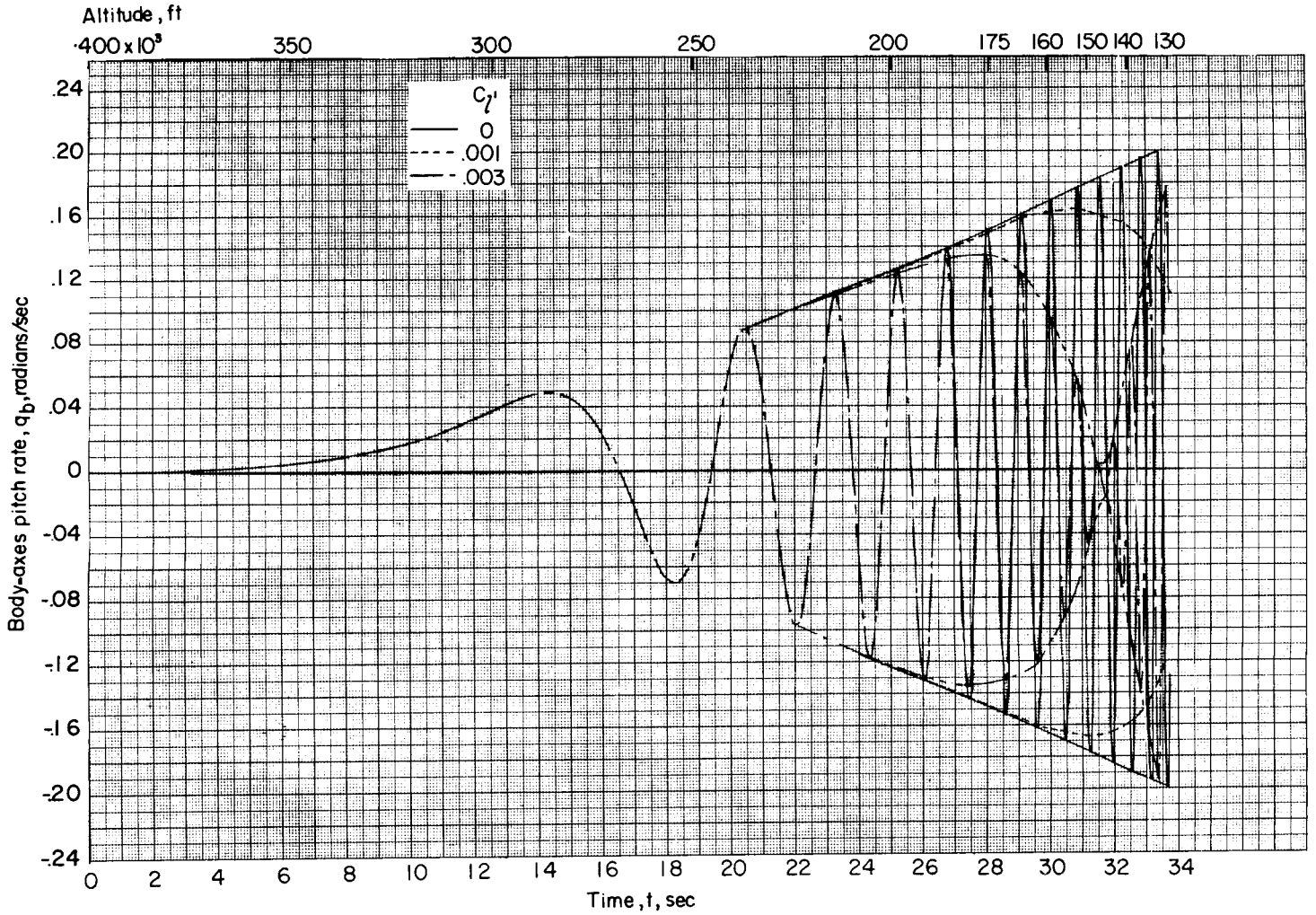

(d) Body-axes pitch-rate time history.

Figure 7.- Continued.

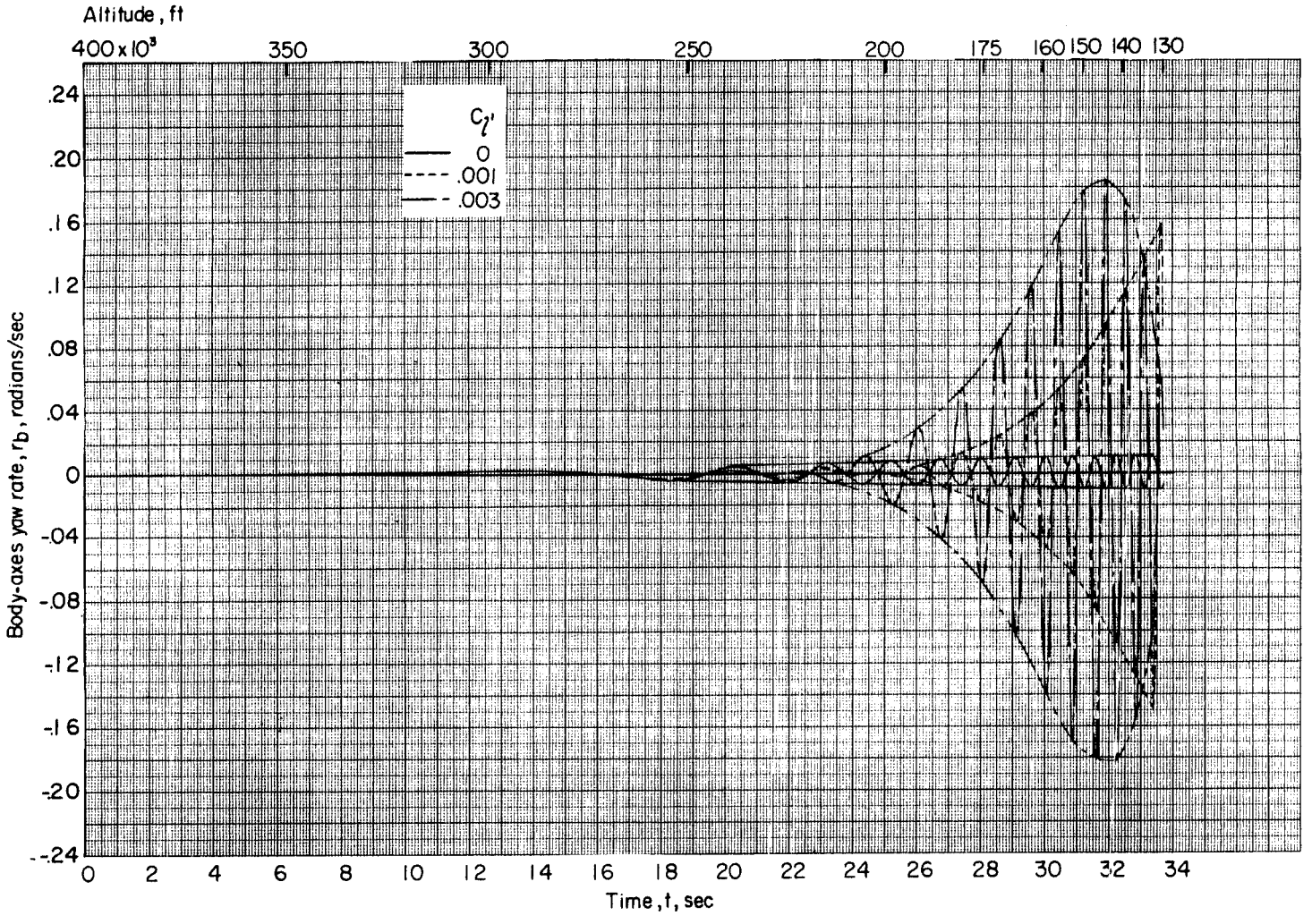

(e) Body-axes yaw-rate time history.

Figure 7.- Concluded.

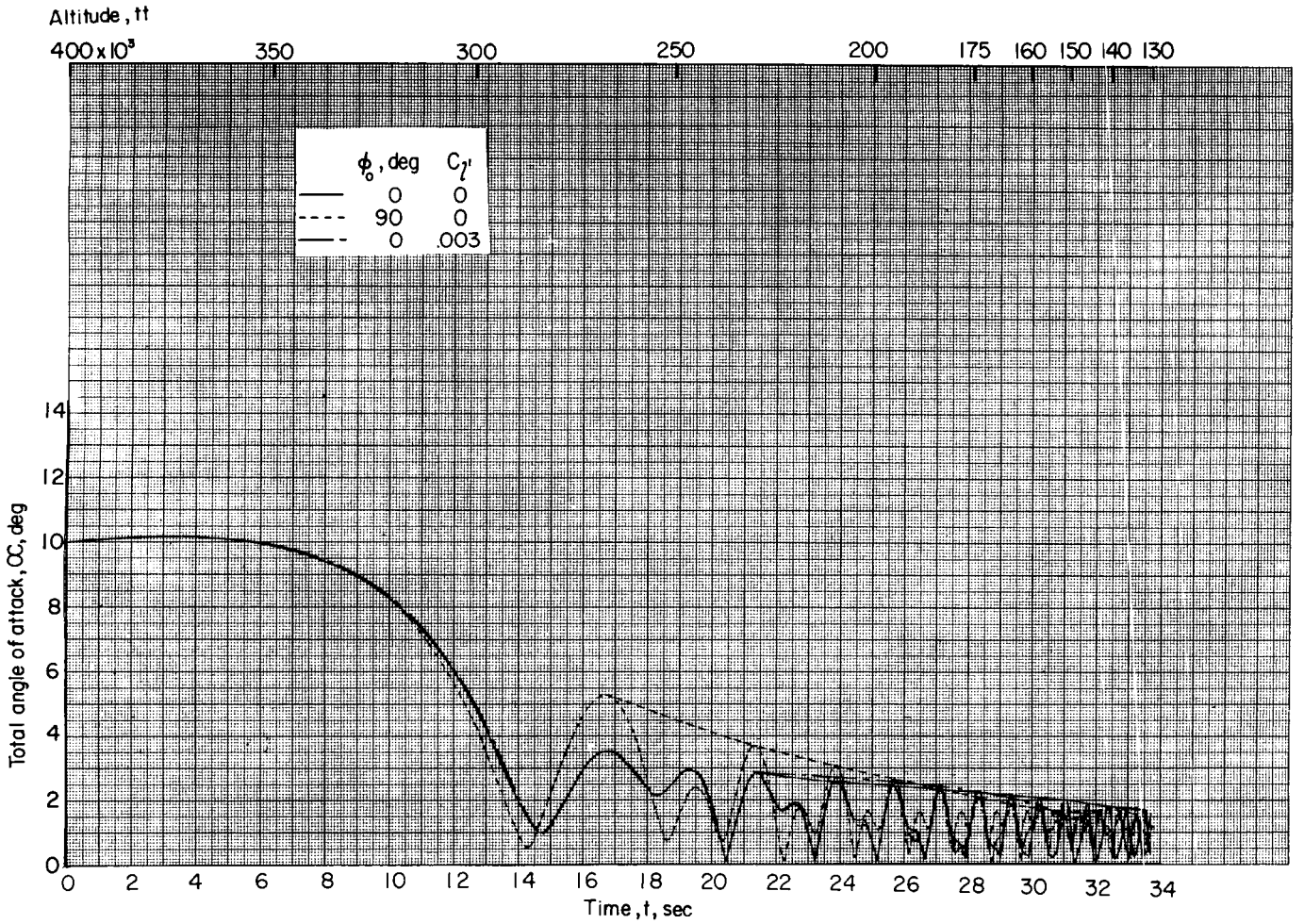

(a) Angle-of-attack time history.

Figure 8.- Effect of initial roll angle and pylon misalinement on time histories. $\alpha_o = 10^o$; $p_o = 10^o$ per second; center-of-gravity offset, 4.9 percent d.

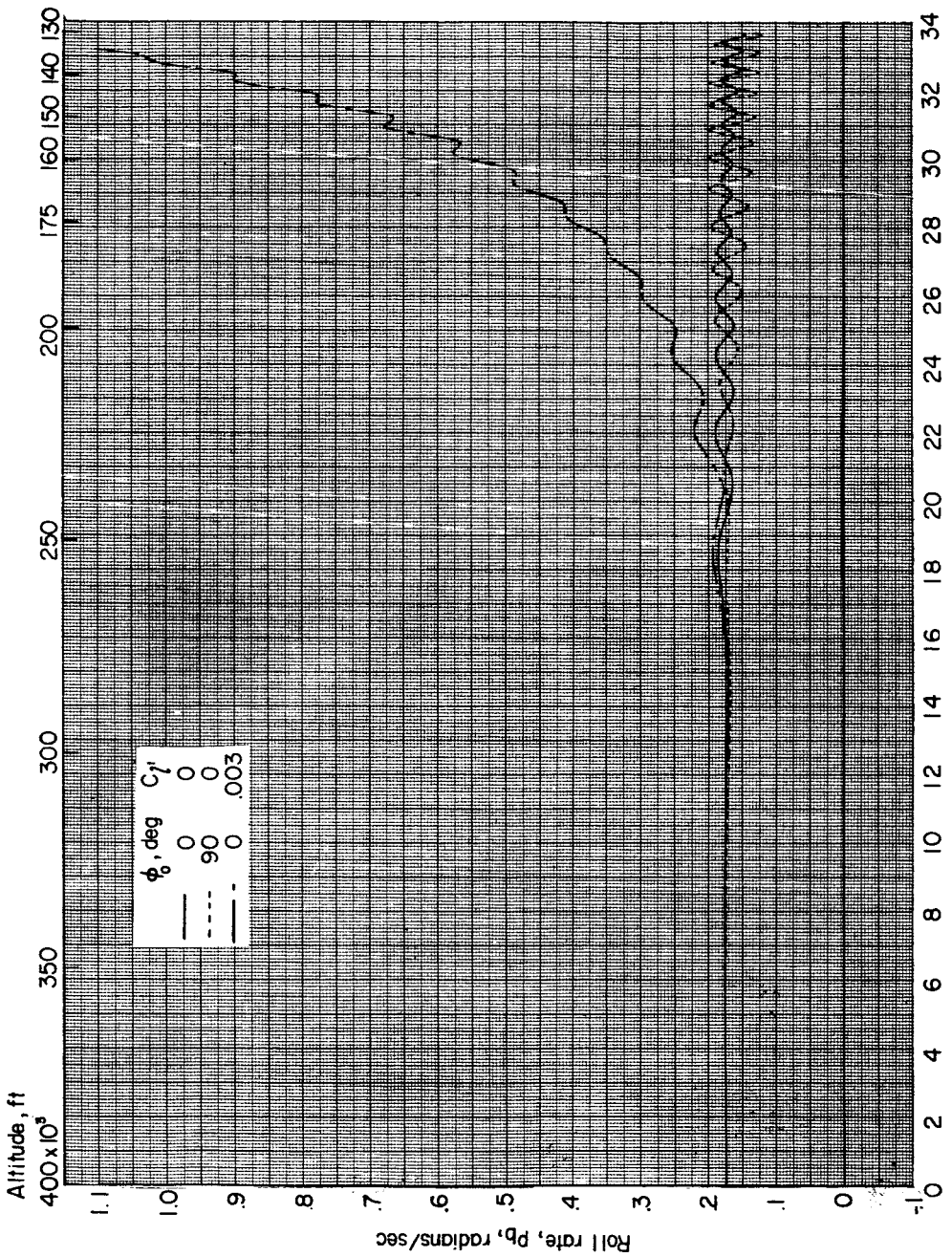

(b) Roll-rate time history.

Figure 8.- Continued.

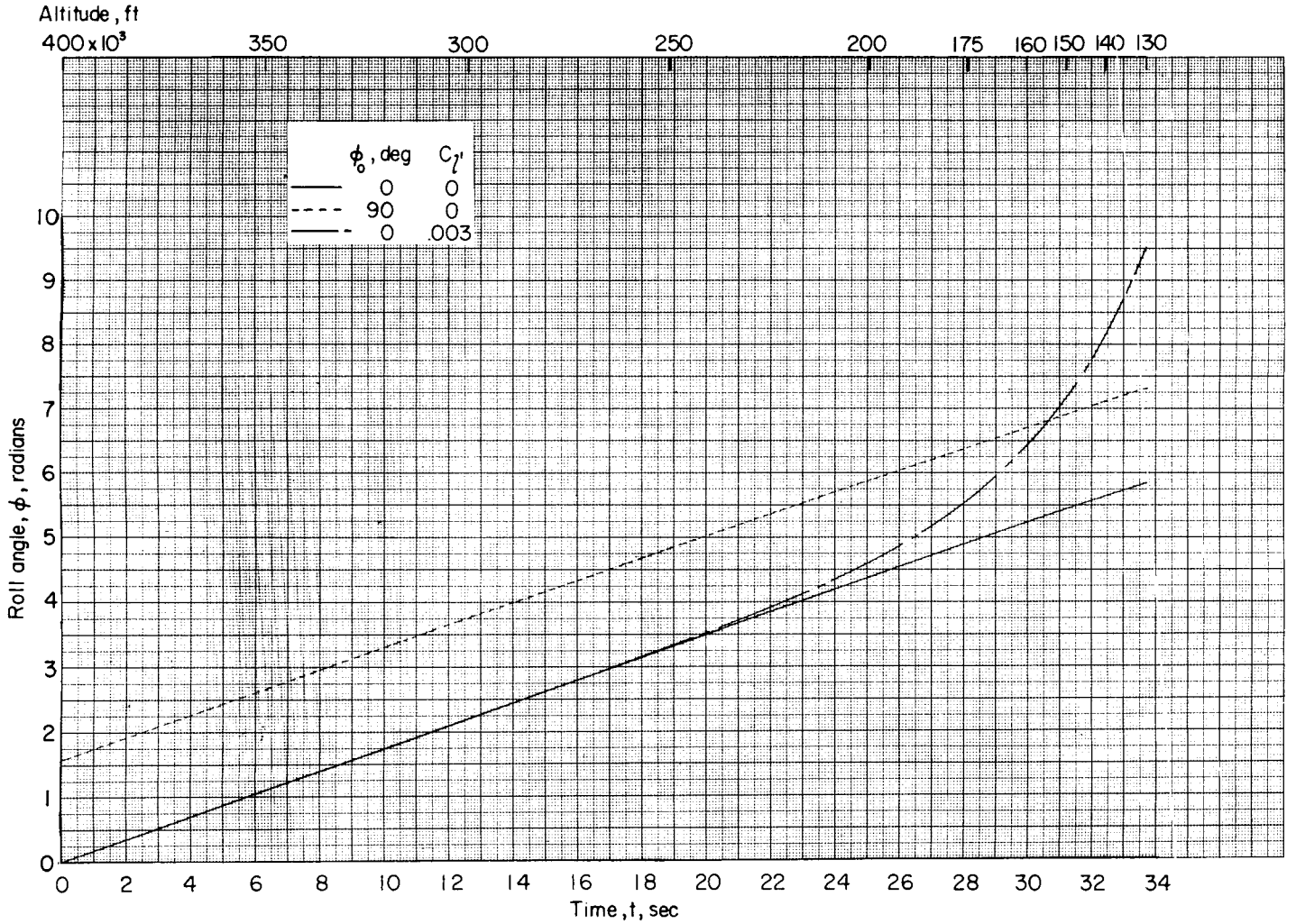

(c) Roll-angle time history.

Figure 8.- Continued.

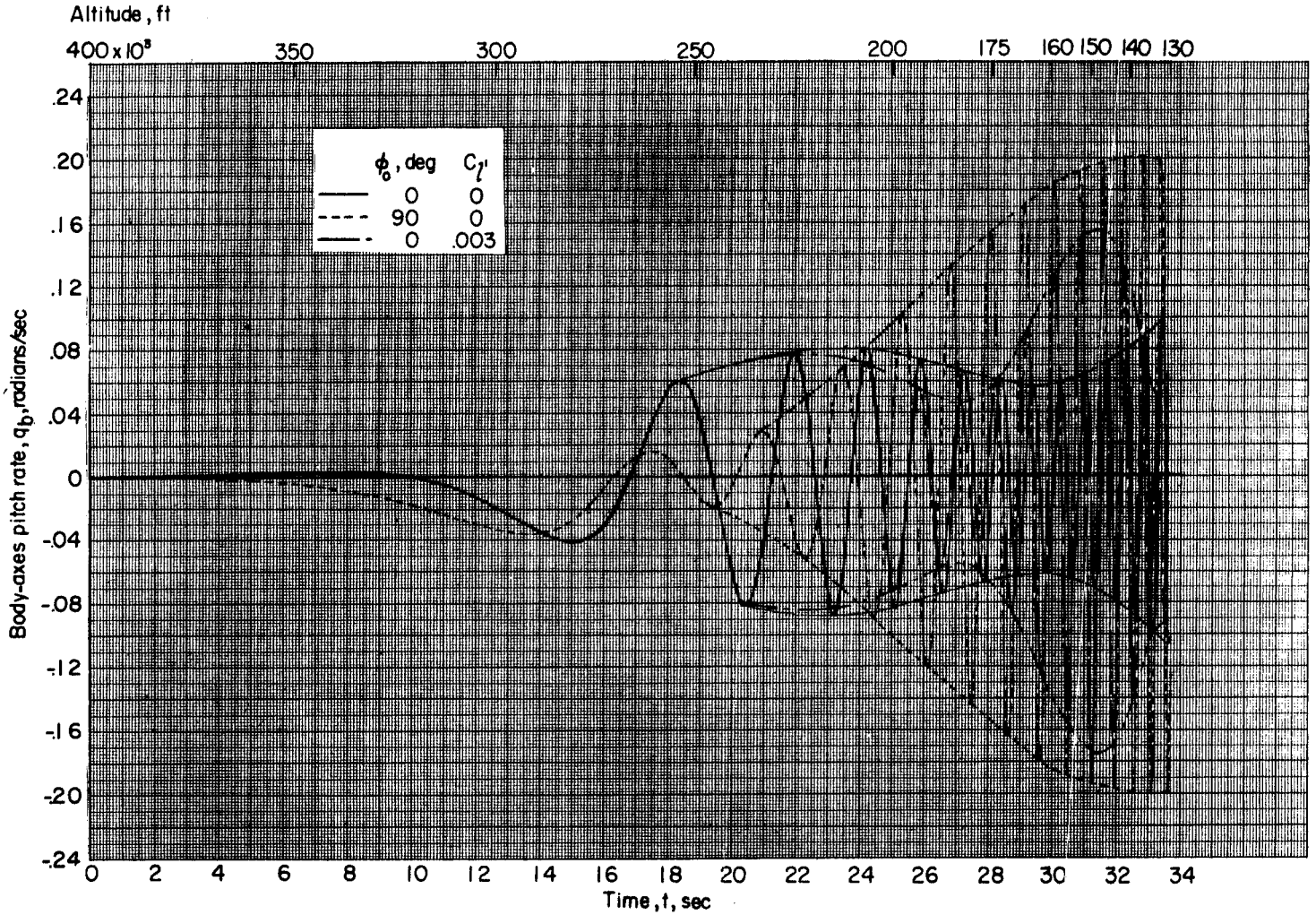

(d) Body-axes pitch-rate time history.

Figure 8.- Continued.

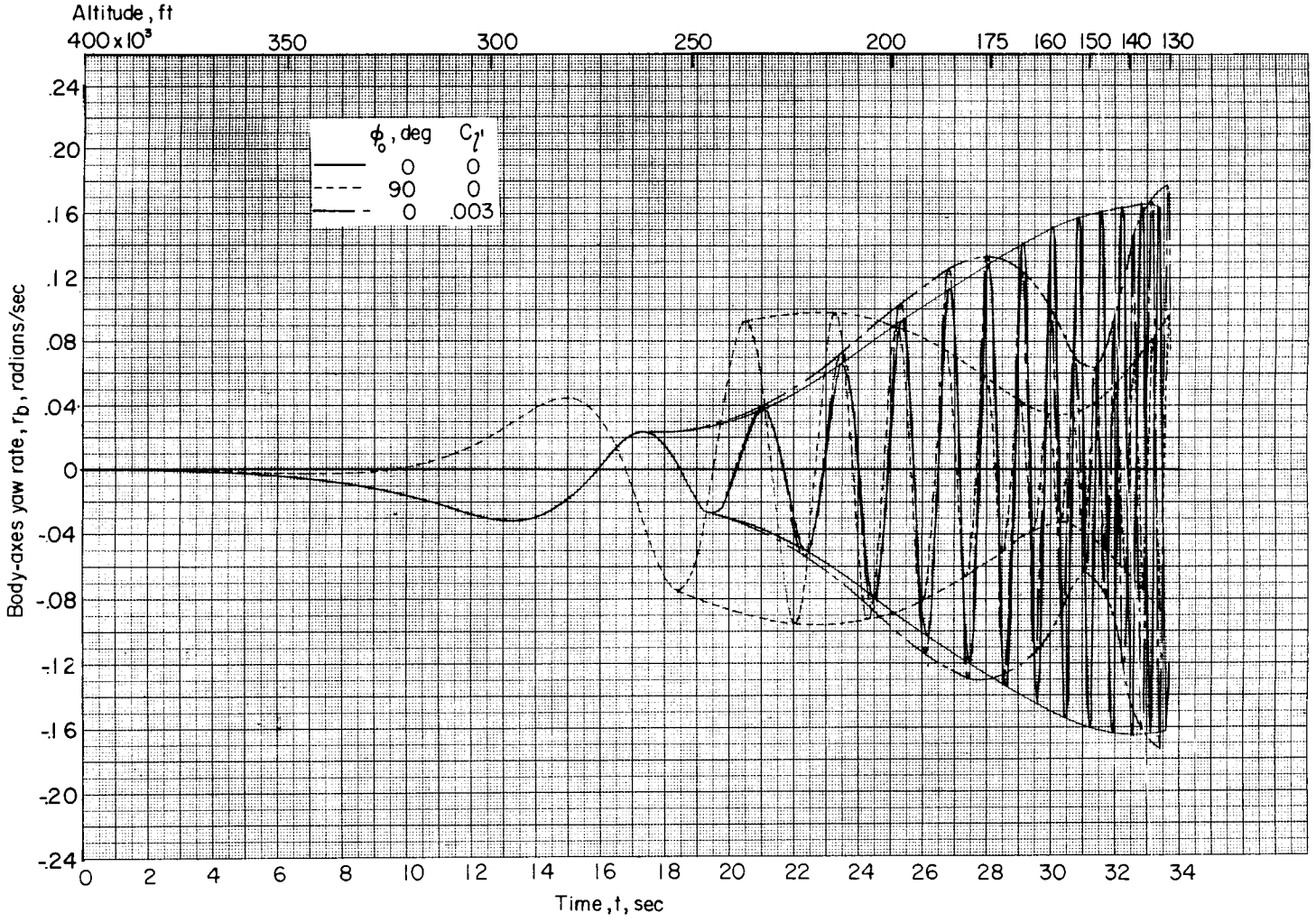

(e) Body-axes yaw-rate time history.

Figure 8.- Concluded.

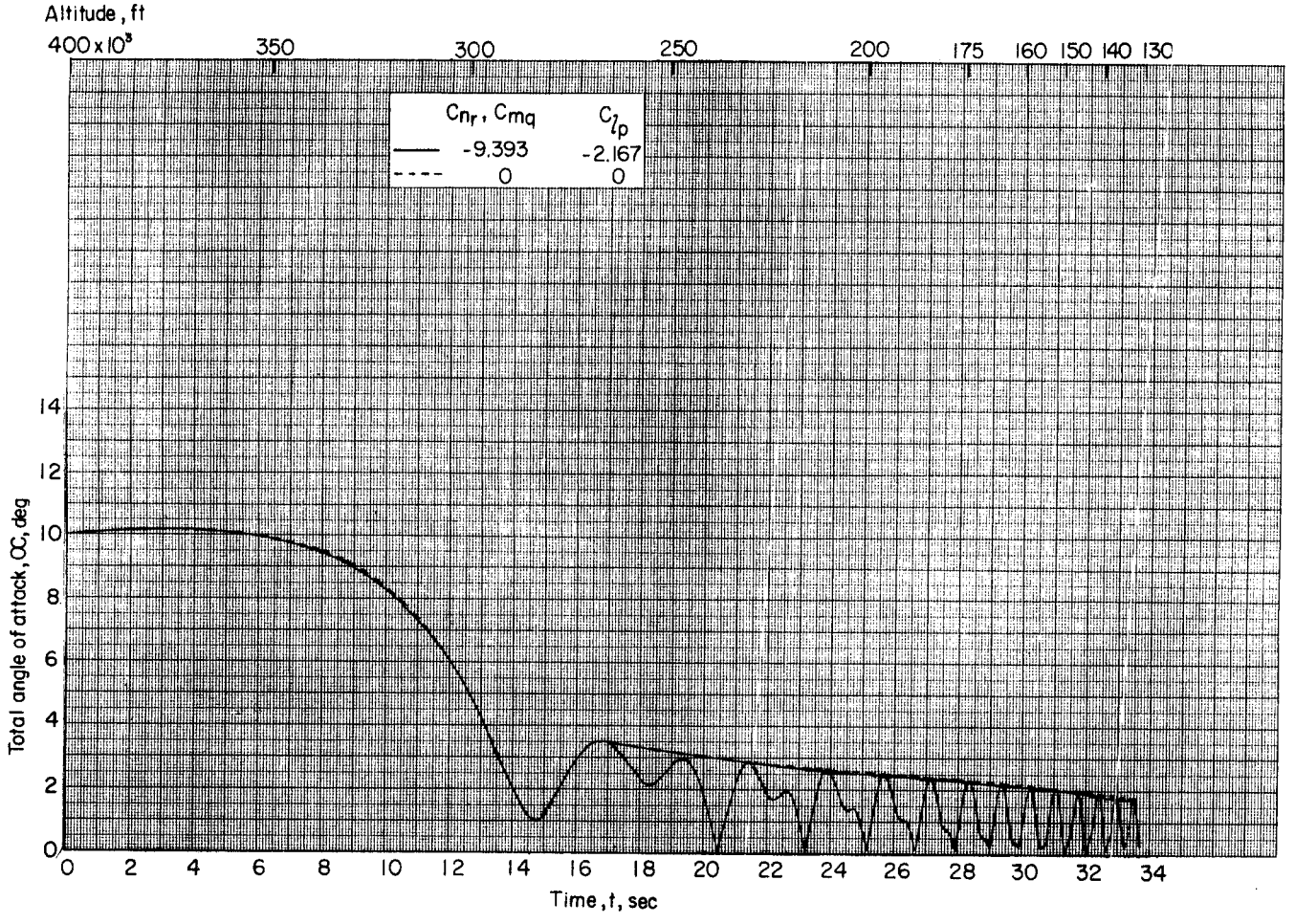

(a) Angle-of-attack time history.

Figure 9.- Effect of damping derivatives on time histories. $\alpha_o = 10^o$; $p_o = 10^o$ per second; center-of-gravity offset, 4.9 percent d; $C_l' = 0$.

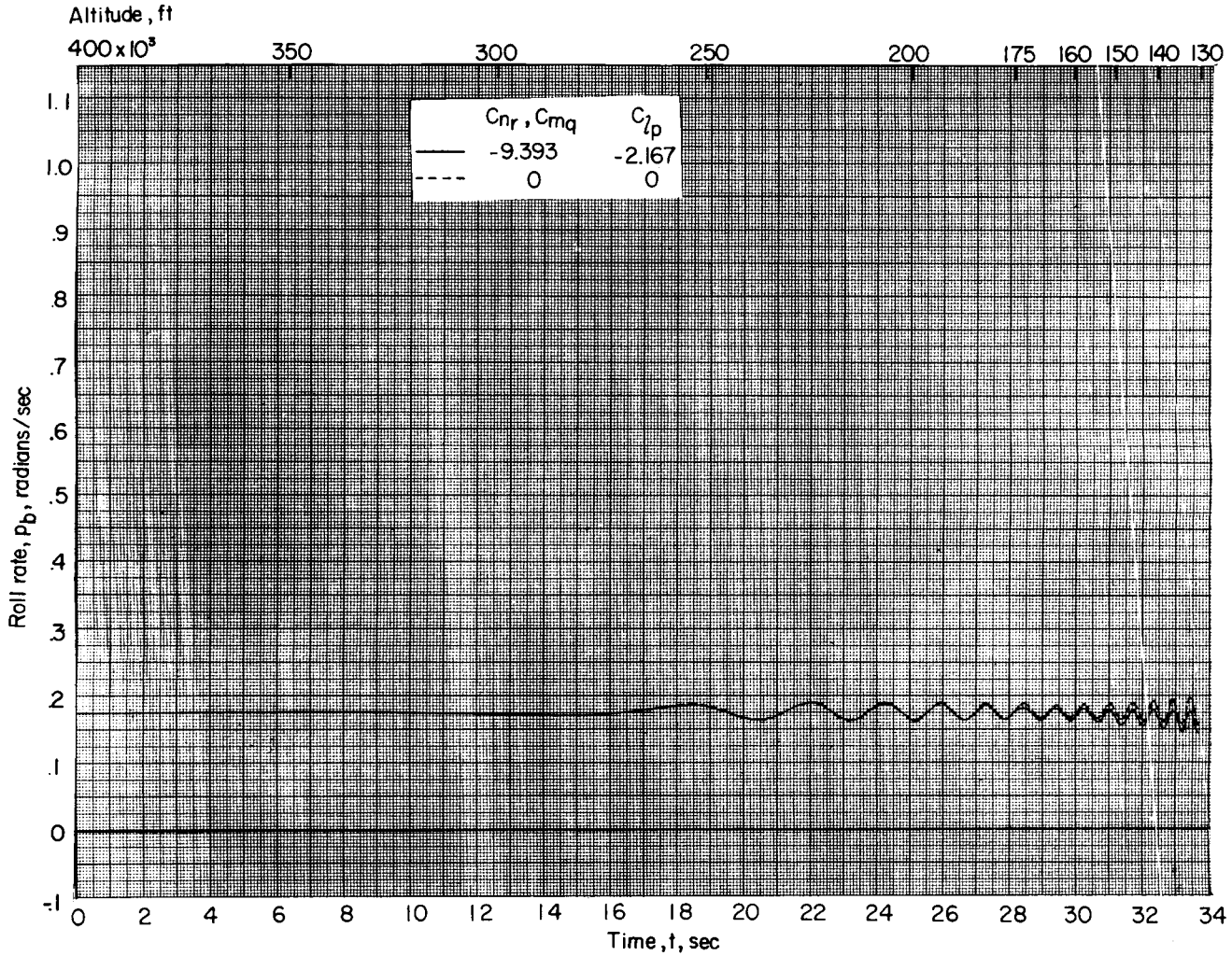

(b) Roll-rate time history.

Figure 9.- Continued.

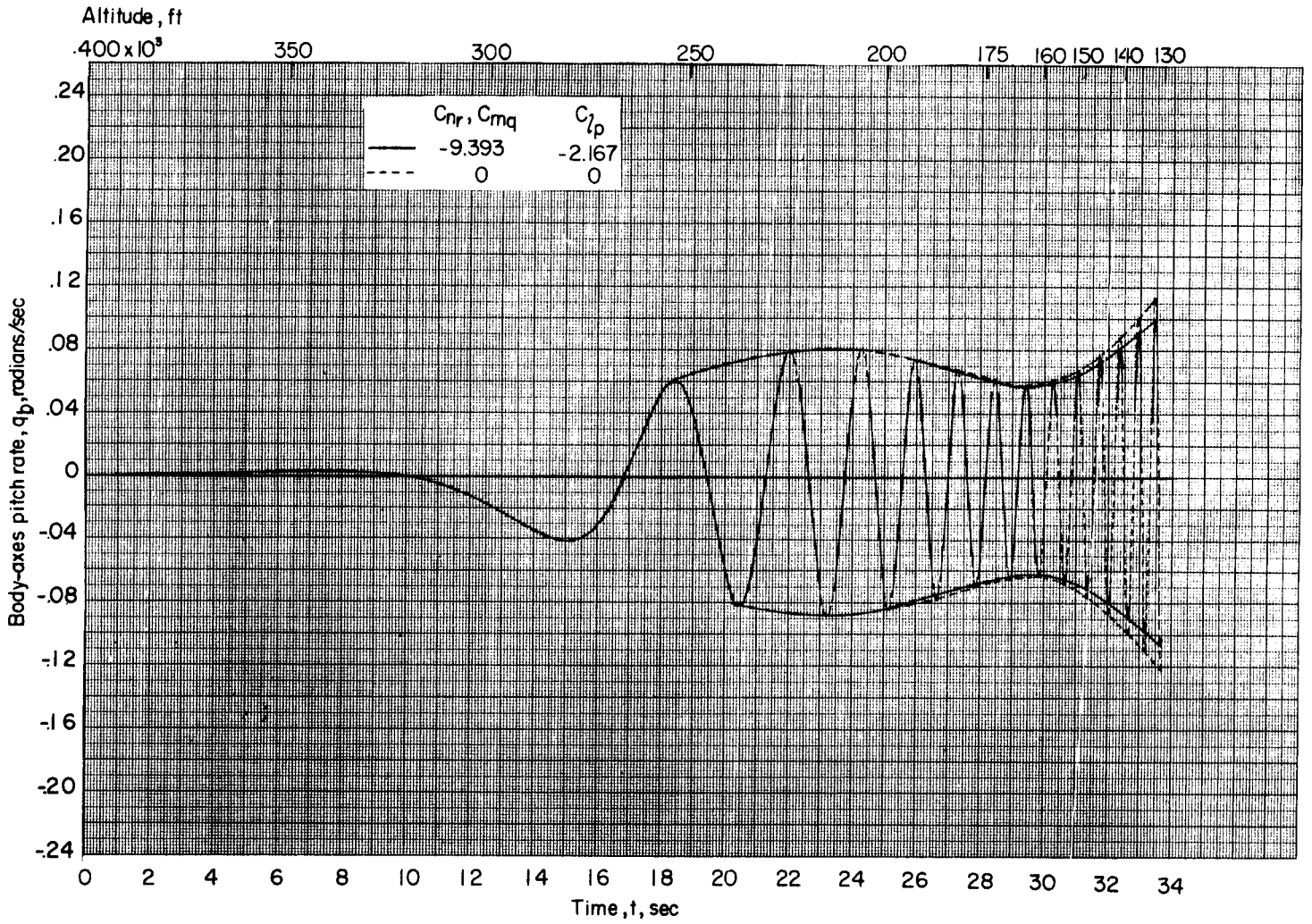

(c) Body-axes pitch-rate time history.

Figure 9.- Continued.

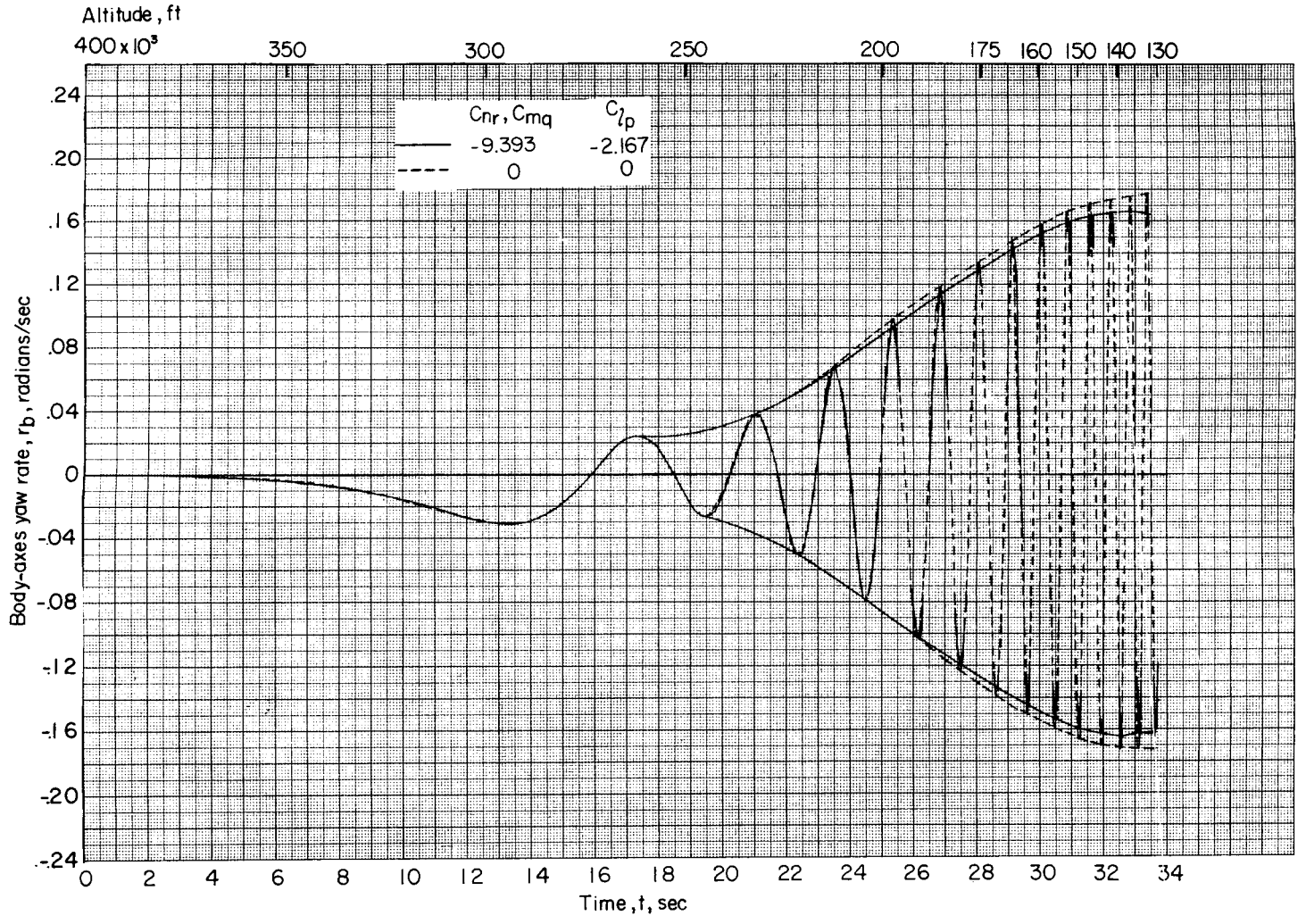

(d) Body-axes yaw-rate time history.

Figure 9.- Concluded.

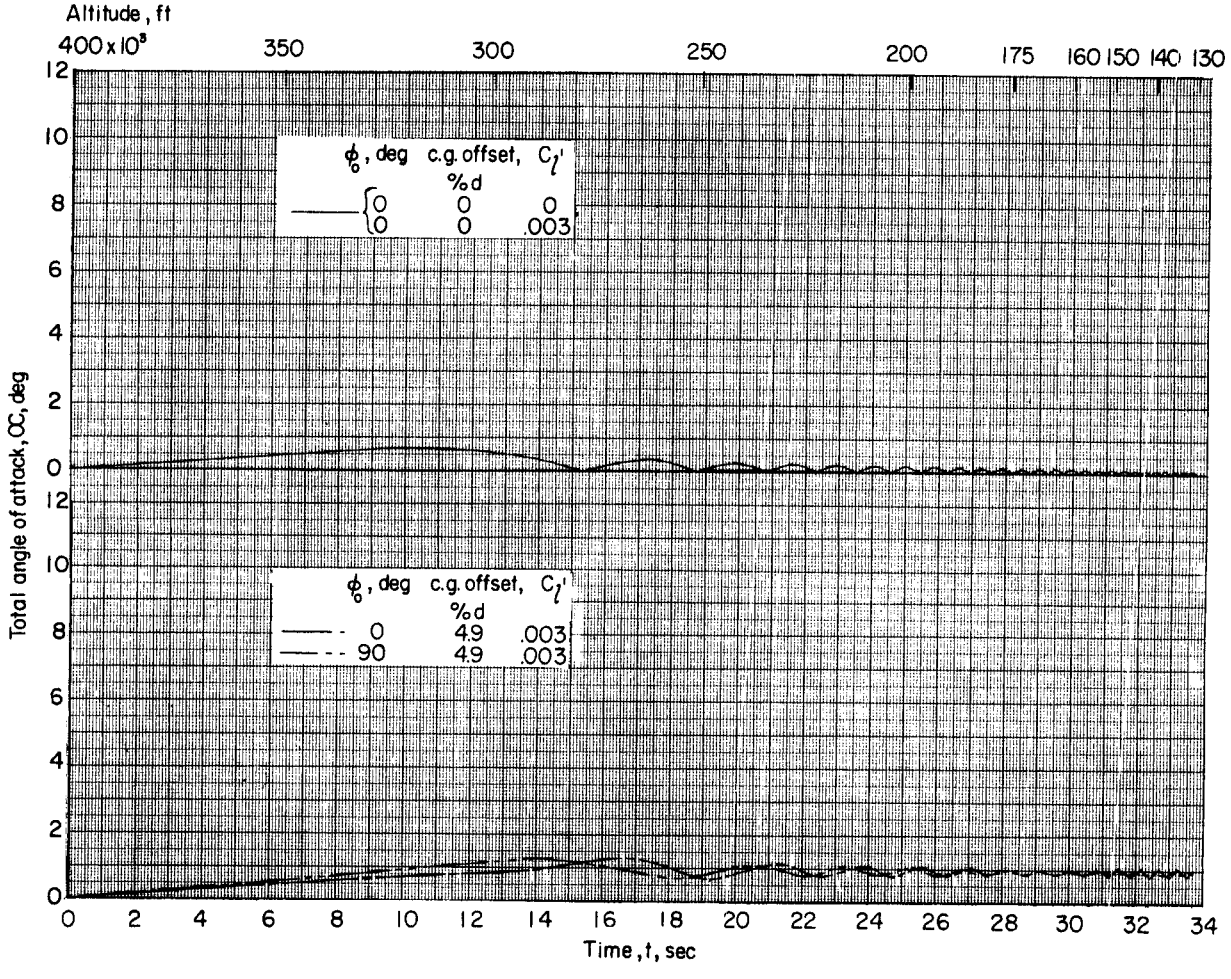

(a) Angle-of-attack time history.

Figure 10.- Effect of pylon misalinement, center-of-gravity offset, and initial roll angle on time histories. $p_o = 0^\circ$ per second; $\alpha_o = 0^\circ$.

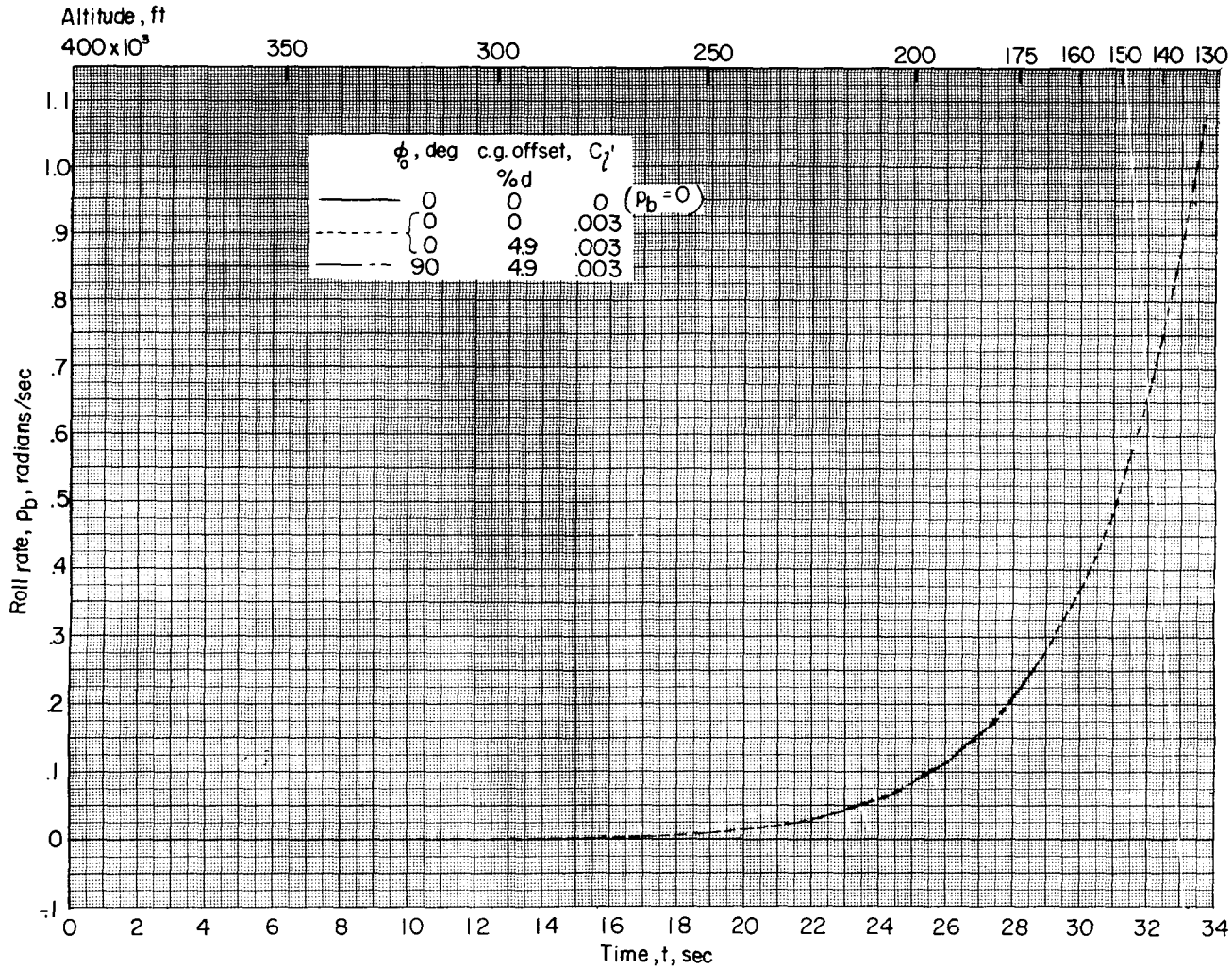

(b) Roll-rate time history.

Figure 10.- Continued.

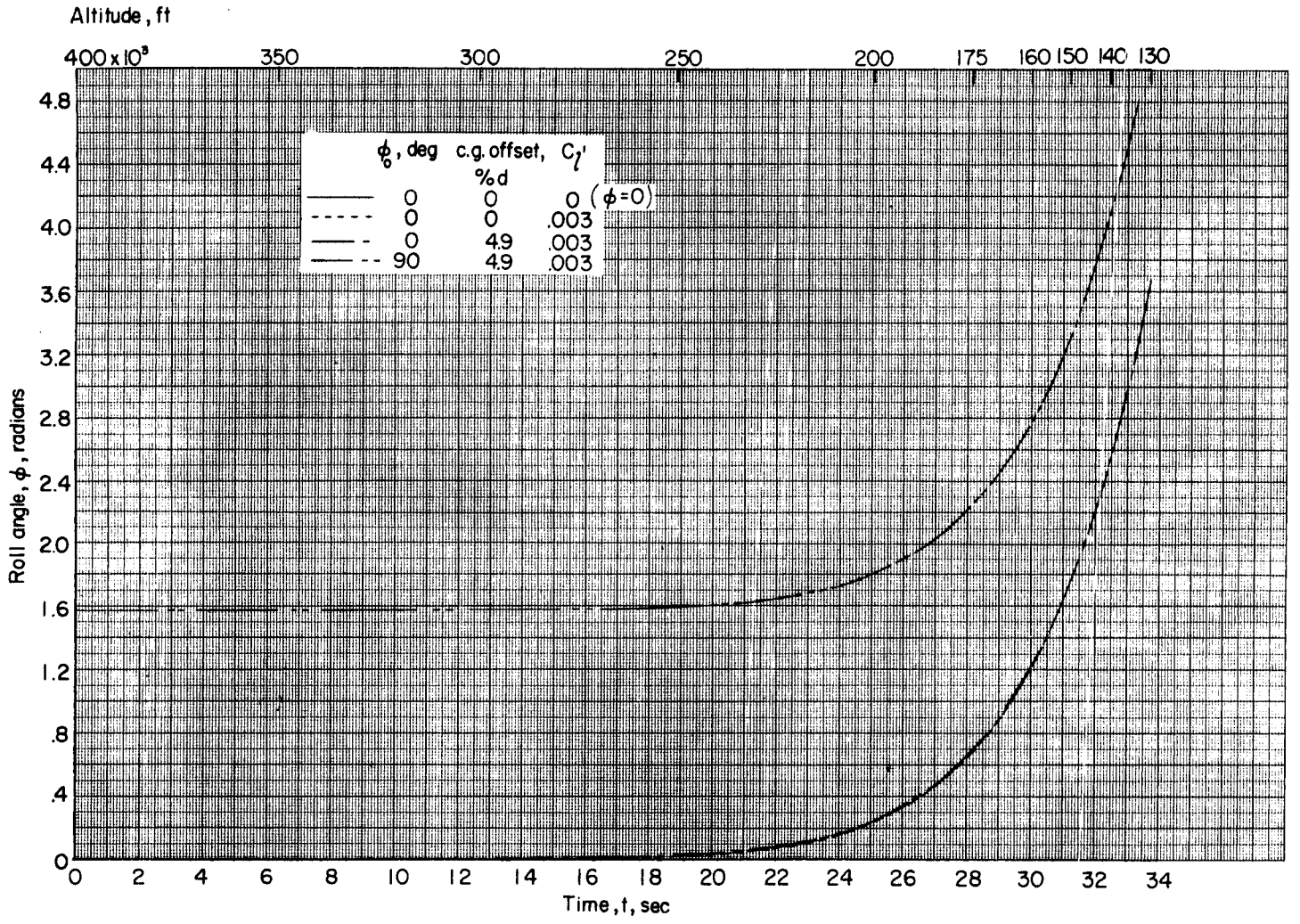

(c) Roll-angle time history.

Figure 10.- Continued.

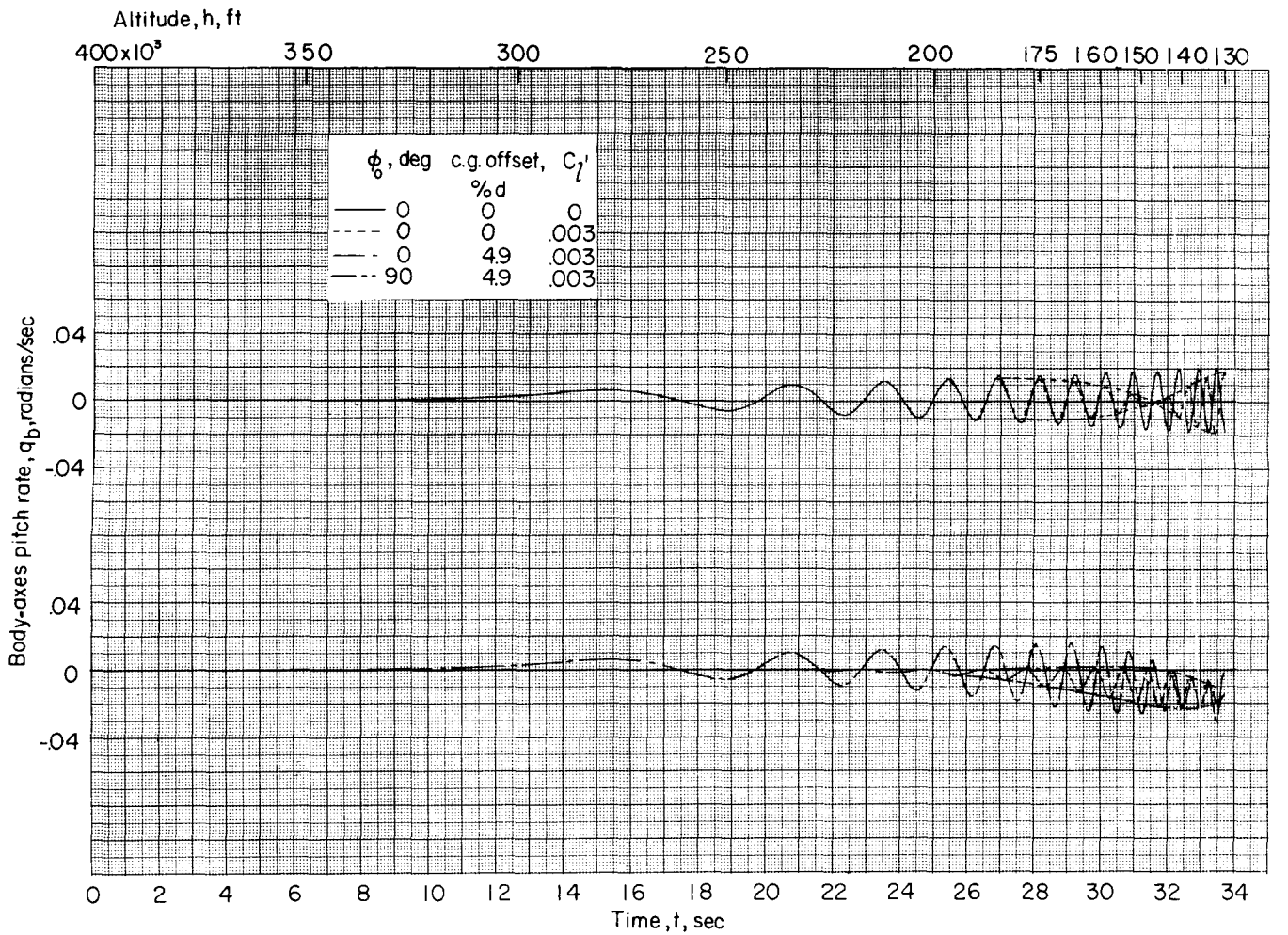

(d) Body-axes pitch-rate time history.

Figure 10.- Continued.

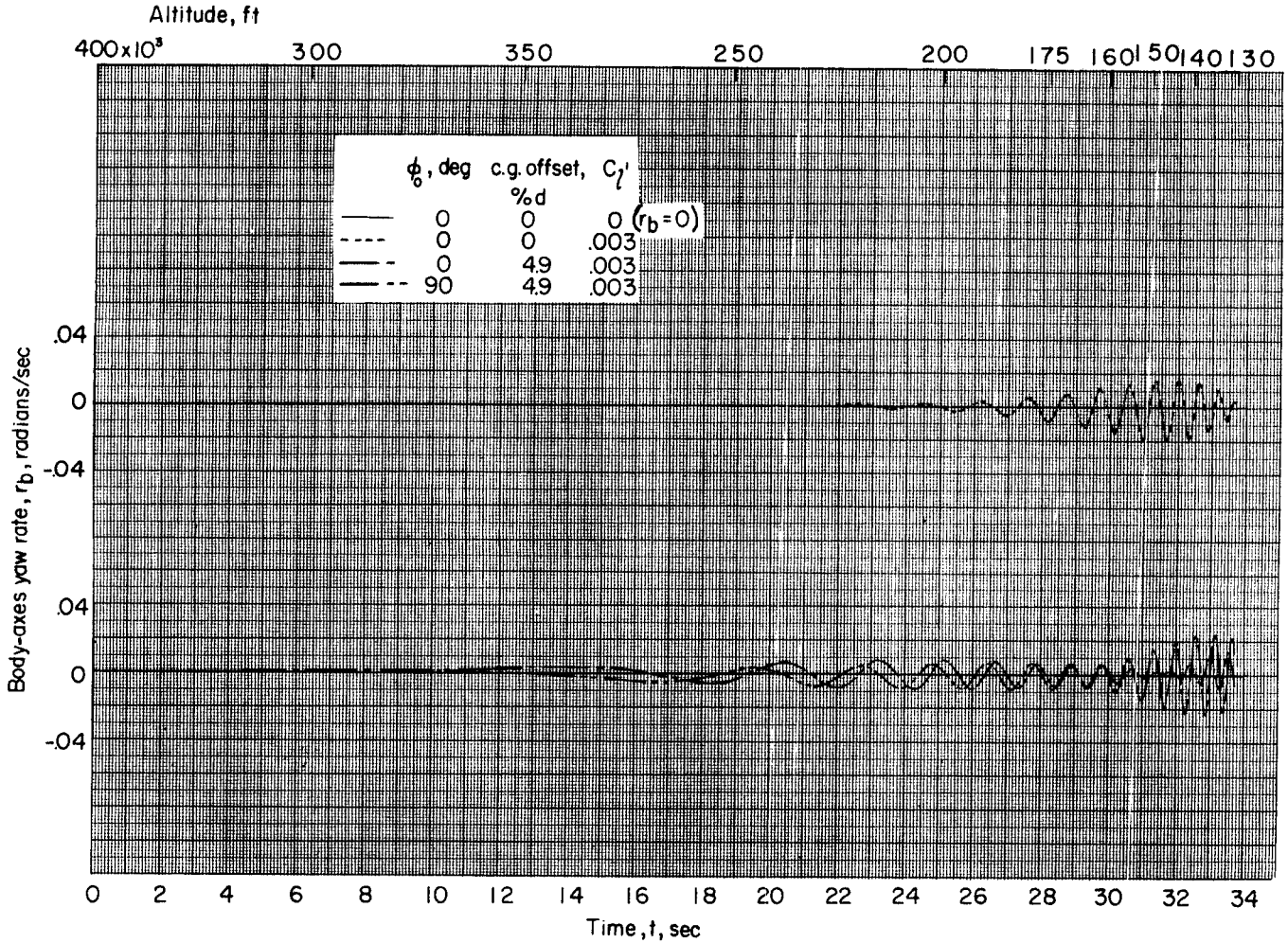

(e) Body-axes yaw-rate time history.

Figure 10.- Concluded.

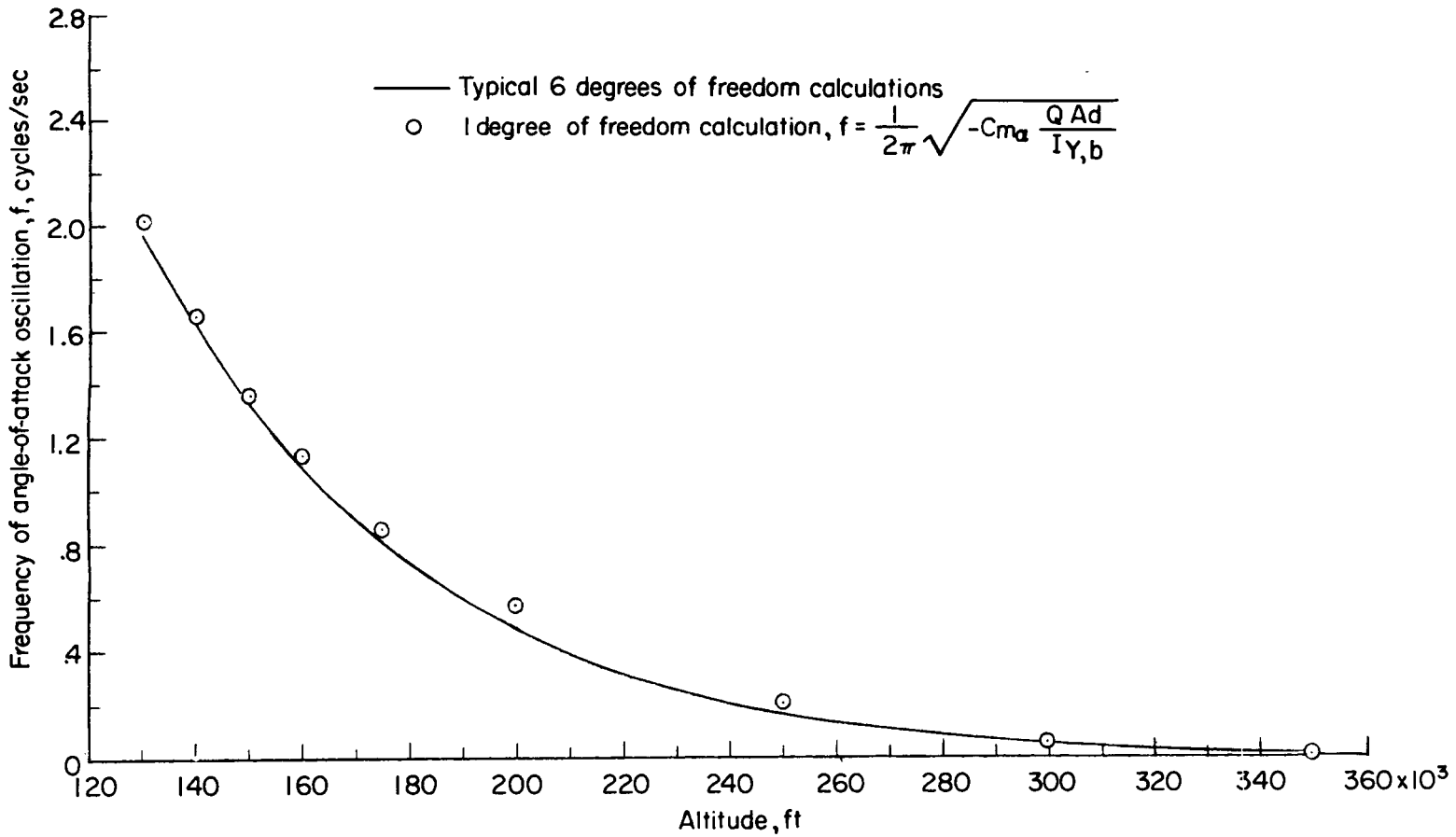

Figure 11.- Comparison of one- and six-degree-of-freedom frequency calculations for angle-of-attack oscillations.

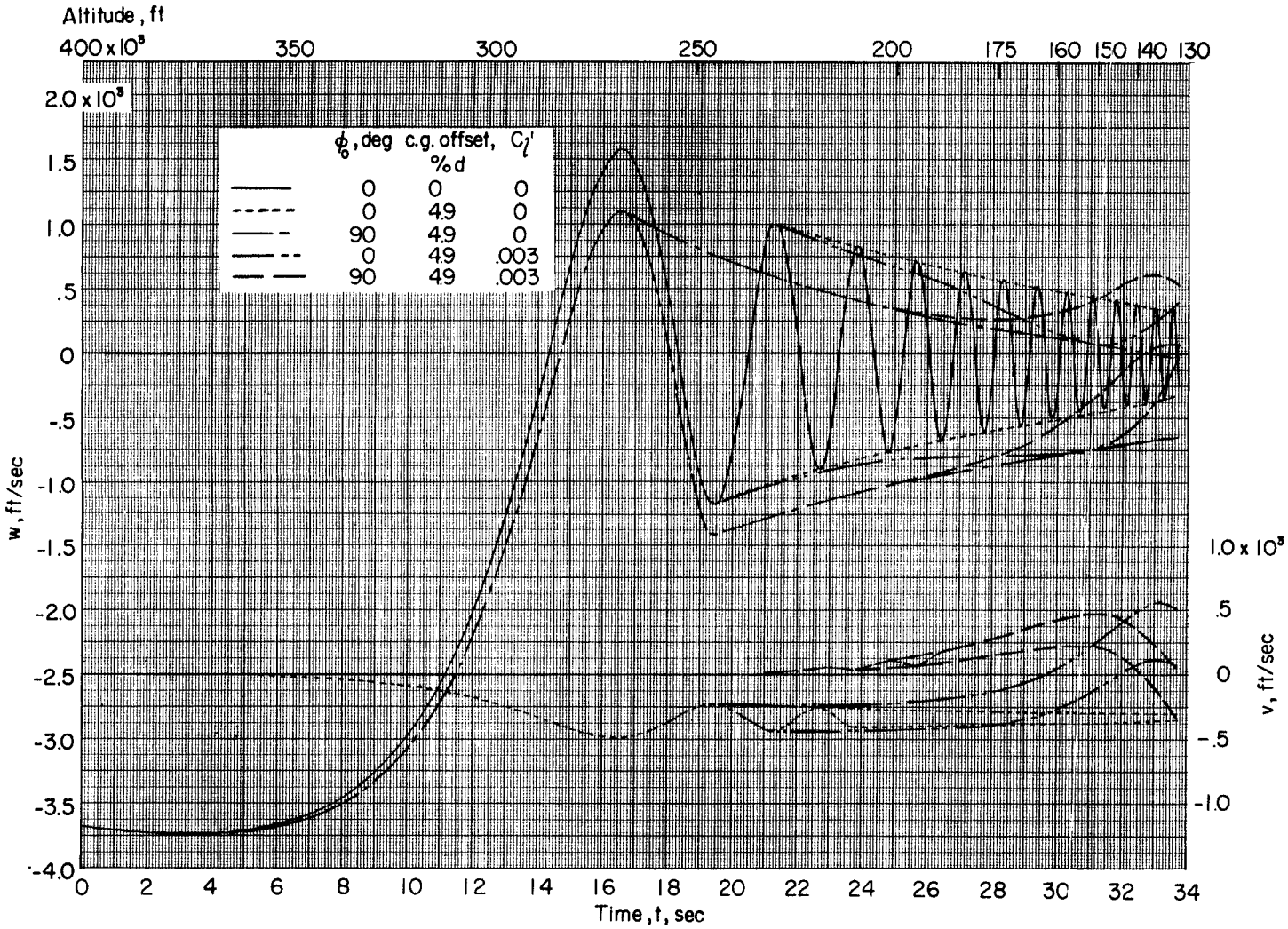

Figure 12.- Time histories of velocities along Y-axis (v) and Z-axis (w) for several reentries. $\alpha_o = 10^o$; $p_o = 0^o$ per second.

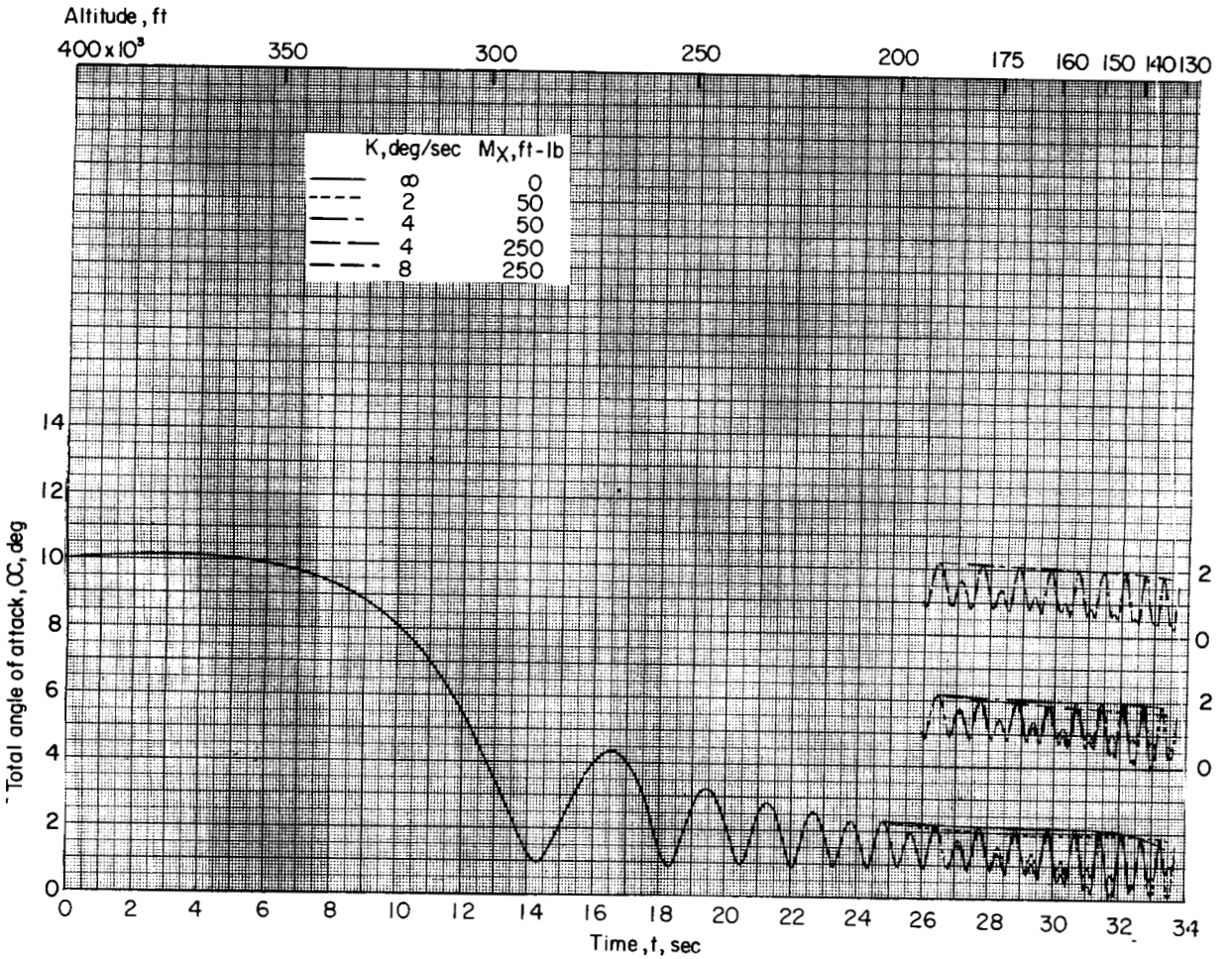

(a) Angle-of-attack time history.

Figure 13.- Effect on time histories of threshold and torque level of a roll-rate control system. $\alpha_o = 10^o$; $p_o = 0^o$ per second; $\phi_o = 0^o$; center-of-gravity offset, 4.9 percent d; $C_l' = 0.003$.

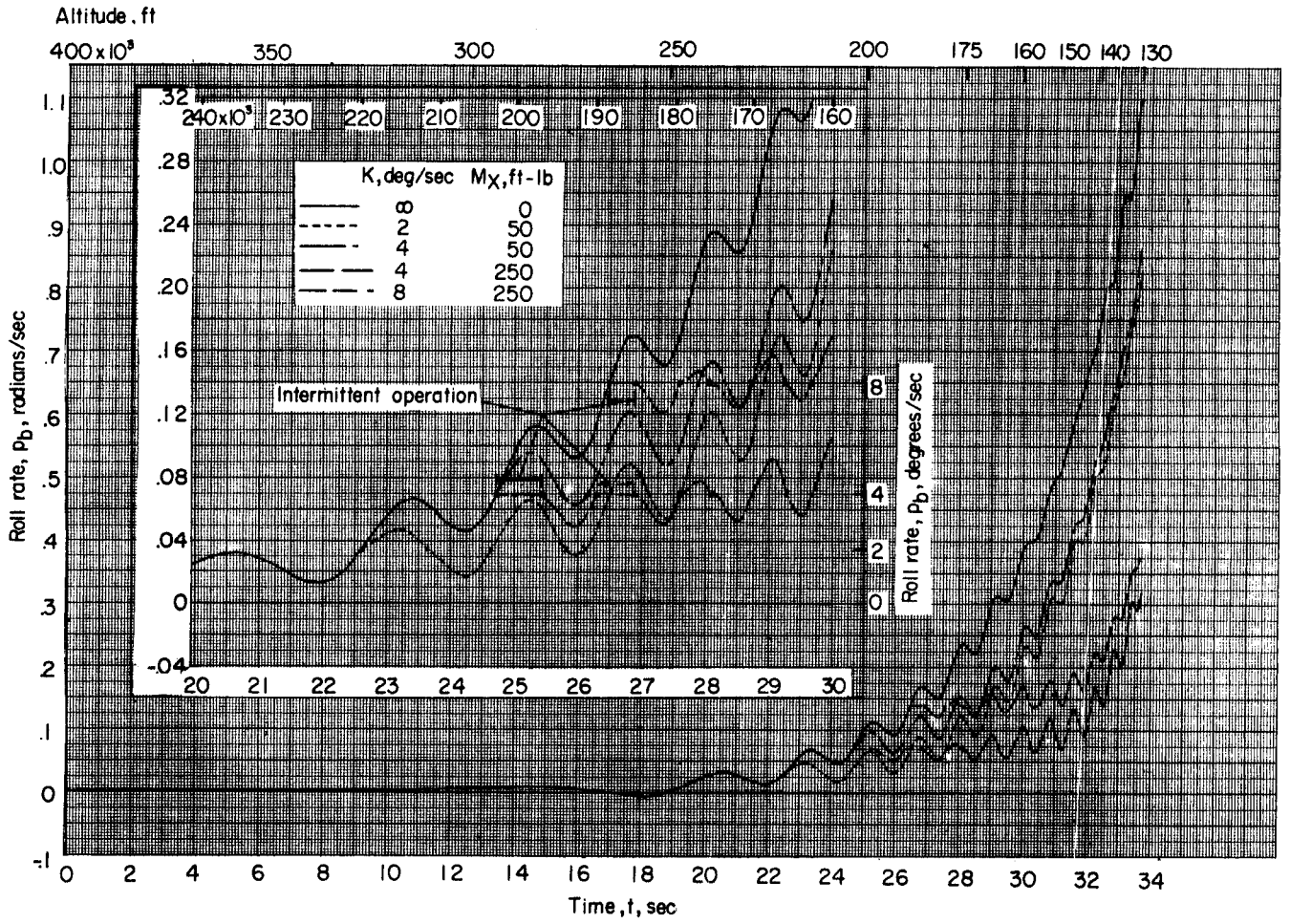

(b) Roll-rate time history. (Tick marks indicate control system operation, on or off. Regions above threshold values not labeled are with continuous control system operation.)

Figure 13.- Continued.

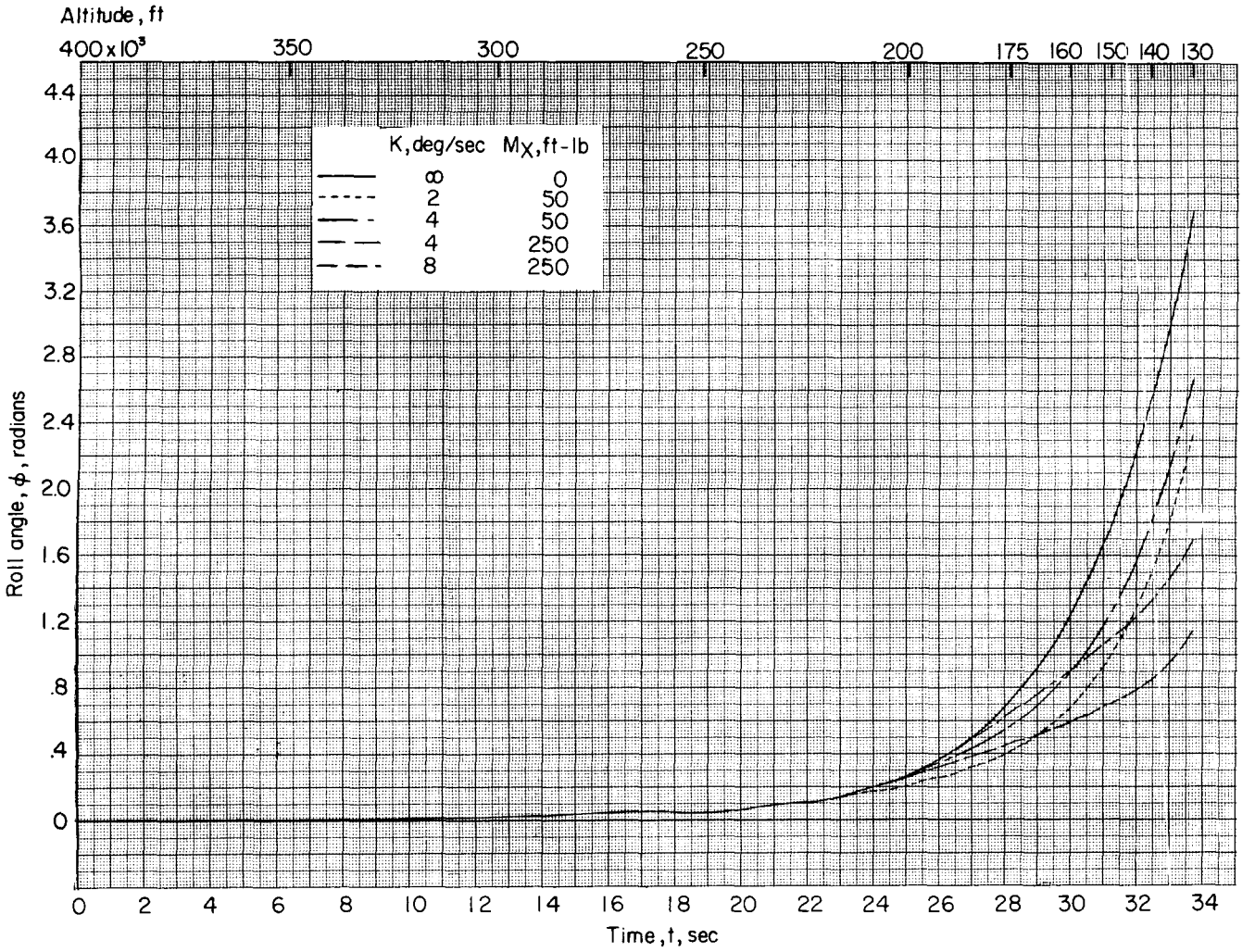

(c) Roll-angle time history.

Figure 13.- Continued.

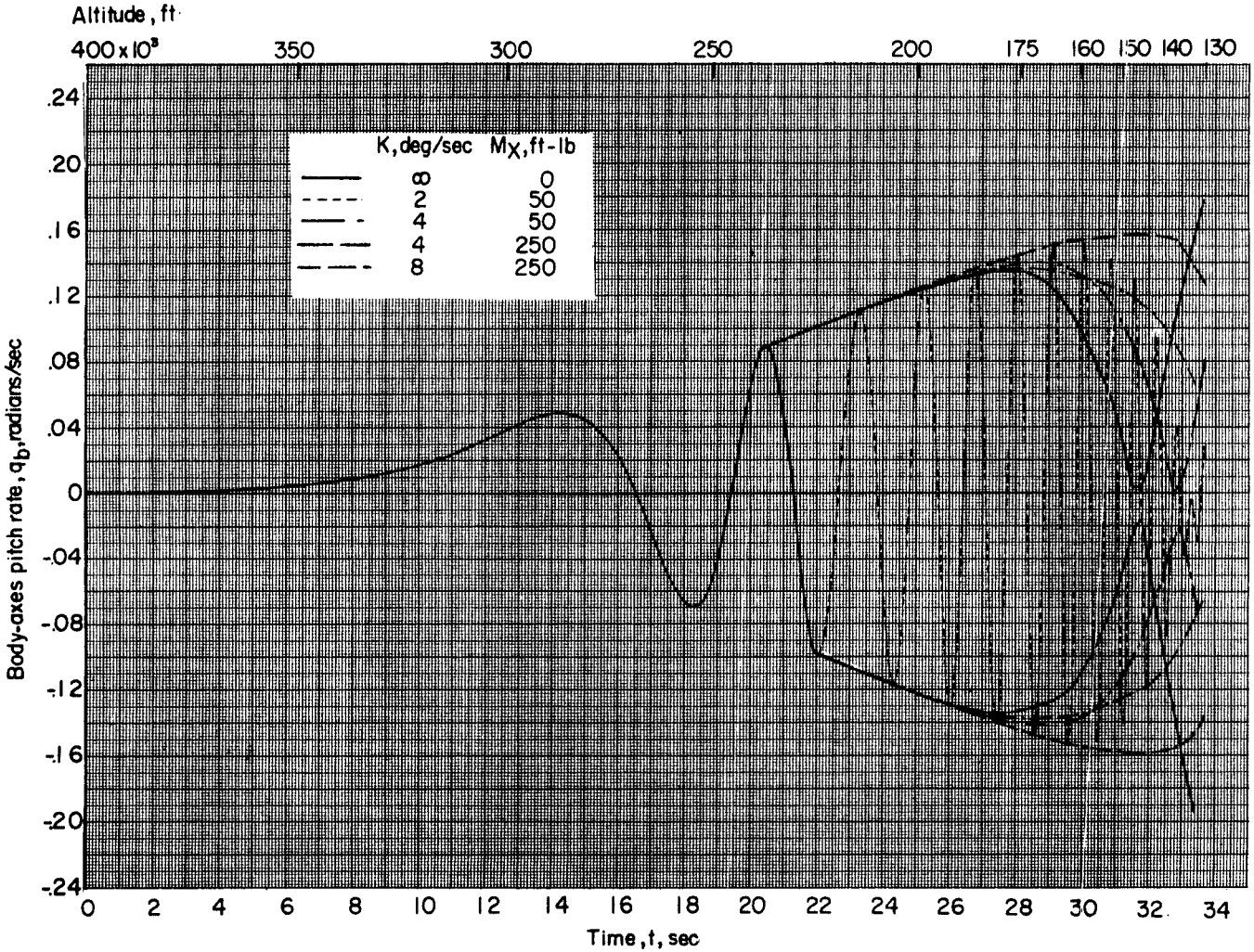

(d) Body-axes pitch-rate time history.

Figure 13.- Continued.

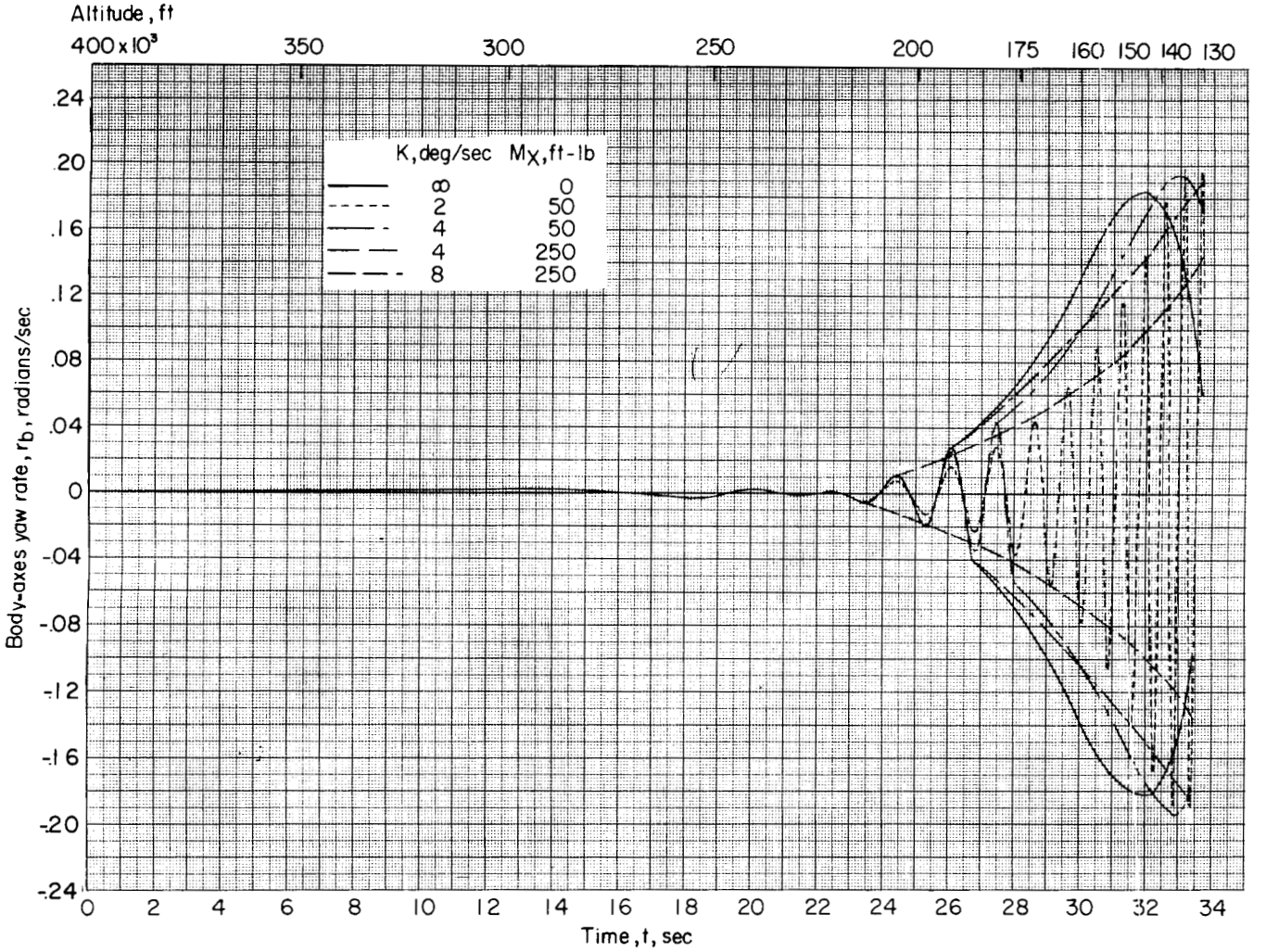

(e) Body-axes yaw-rate time history.

Figure 13.- Concluded.

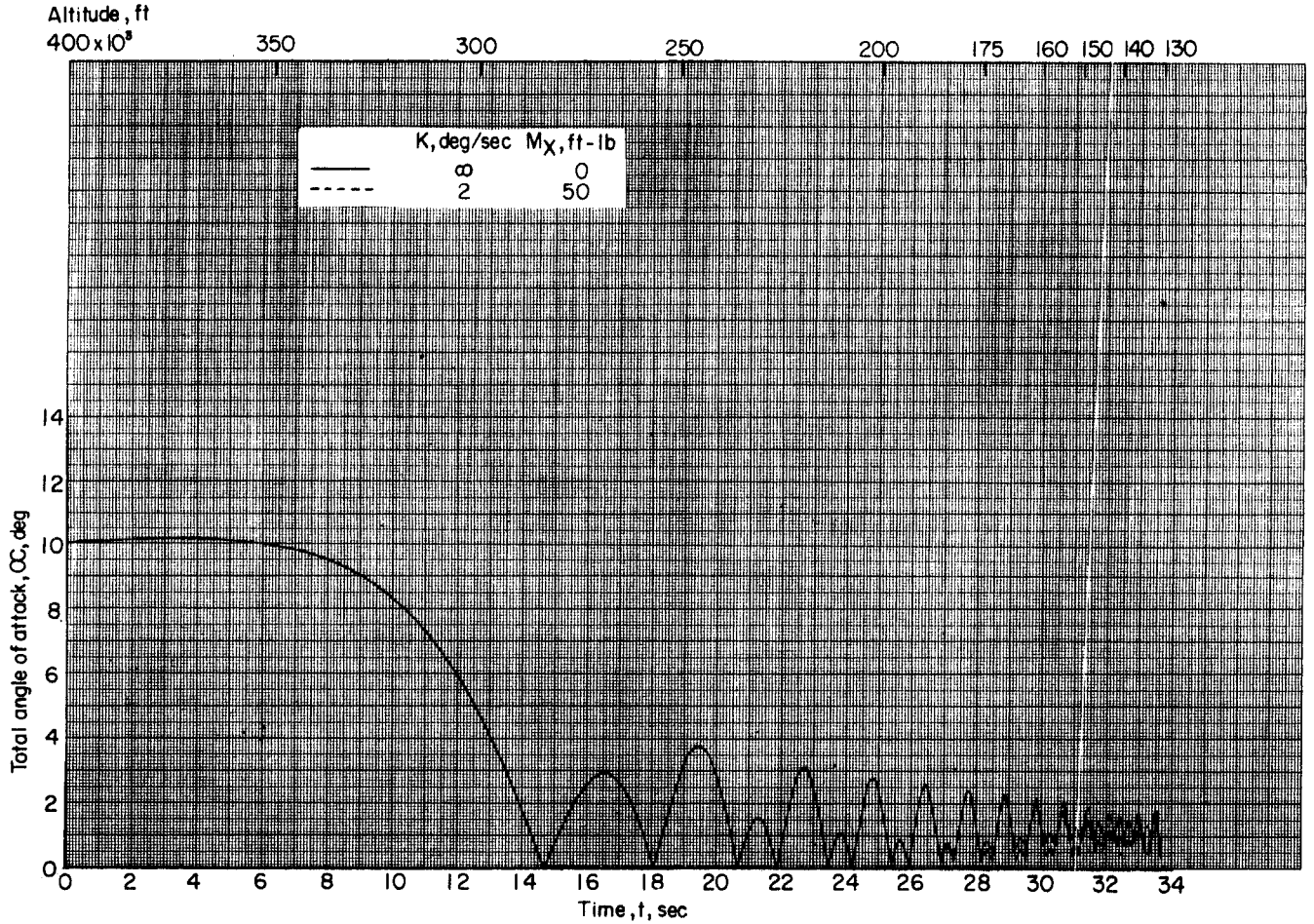

(a) Angle-of-attack time history.

Figure 14.- Effect on time histories of threshold and torque level of a roll-rate control system. $\alpha_o = 10^o$; $p_o = 0^o$ per second; $\phi_o = 90^o$; center-of-gravity offset, 4.9 percent d; $C_l' = 0.003$.

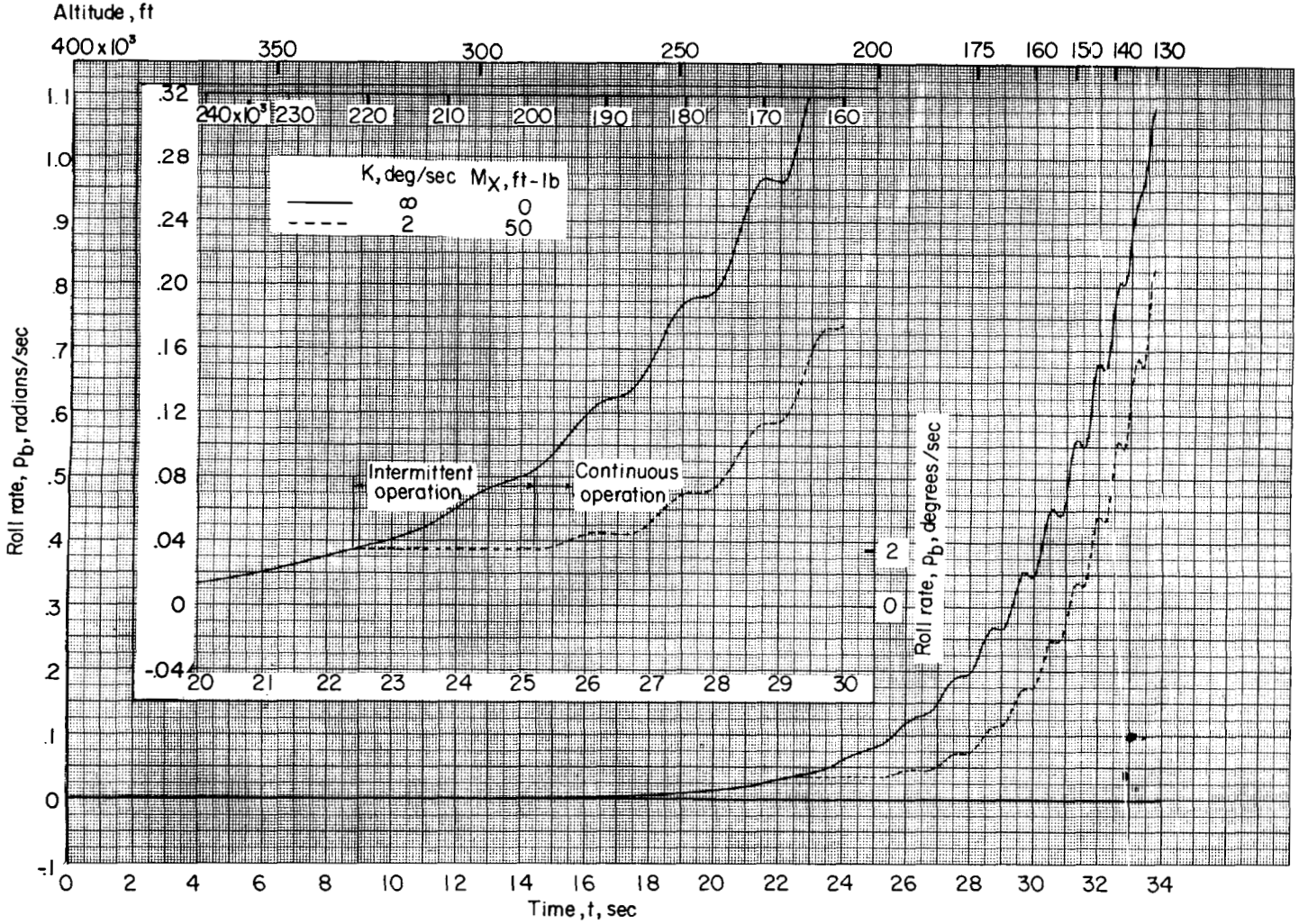

(b) Roll-rate time history.

Figure 14.- Continued.

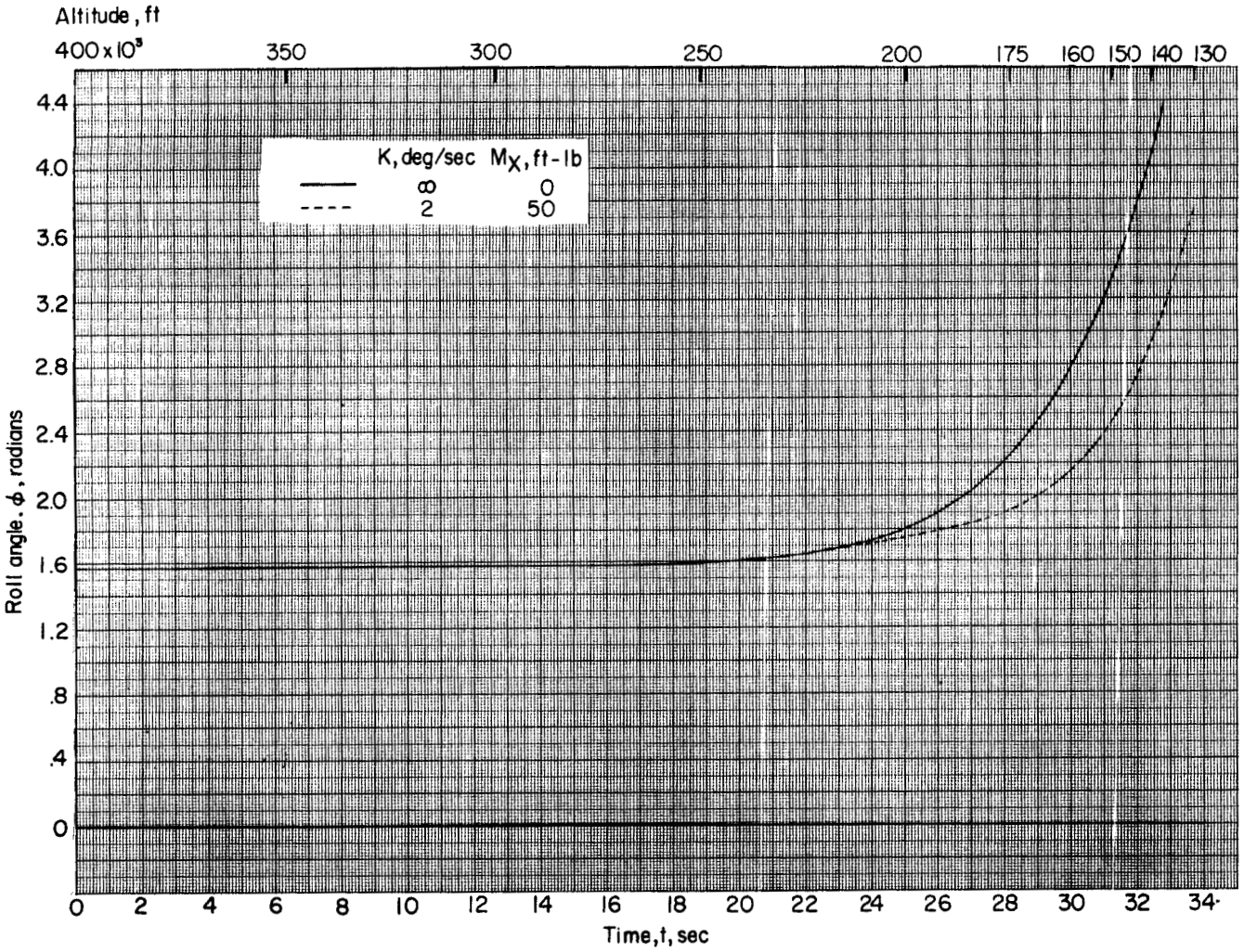

(c) Roll-angle time history.

Figure 14.- Continued.

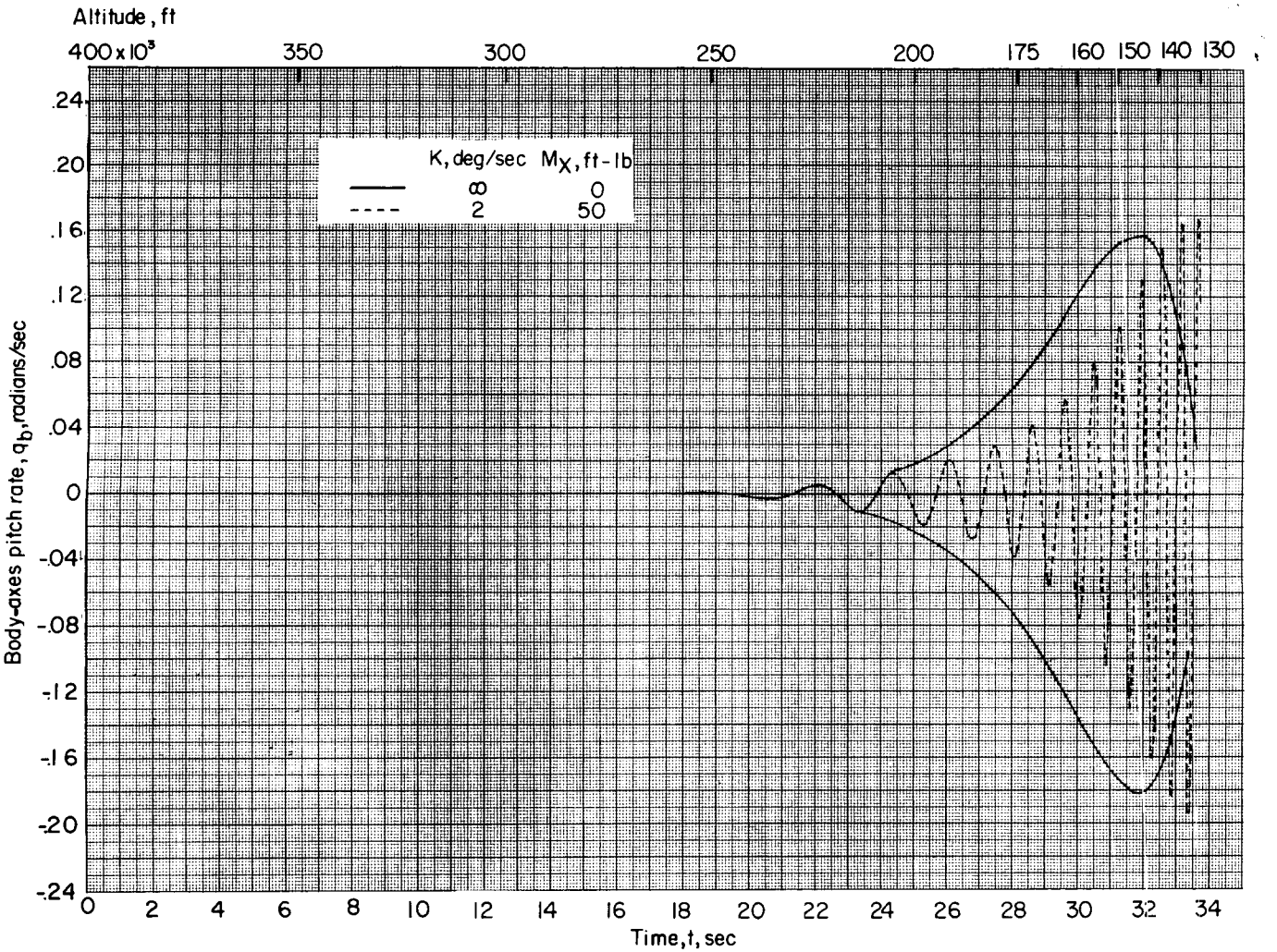

(d) Body-axes pitch-rate time history.

Figure 14.- Continued.

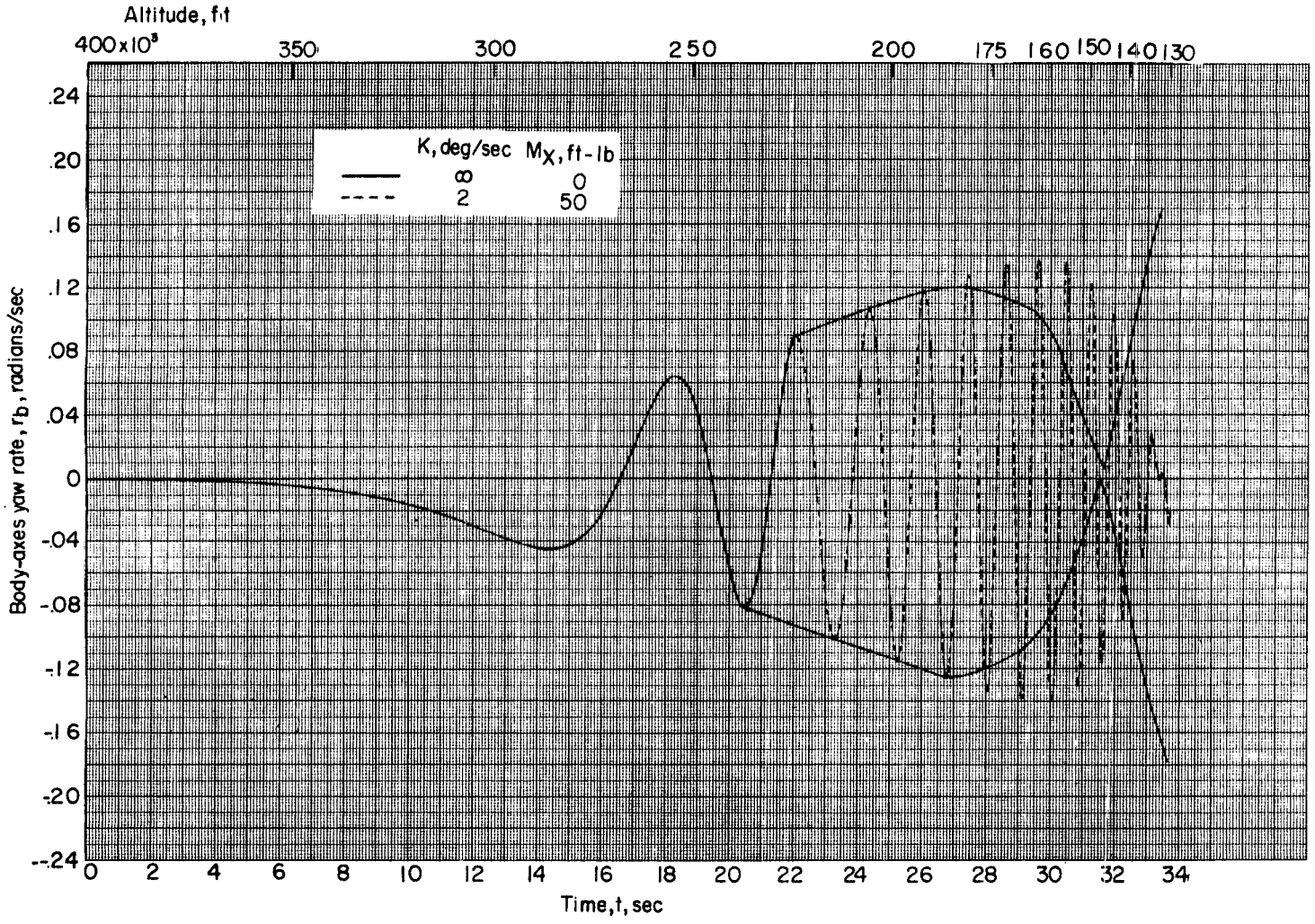

(e) Body-axes yaw-rate time history.

Figure 14.- Concluded.

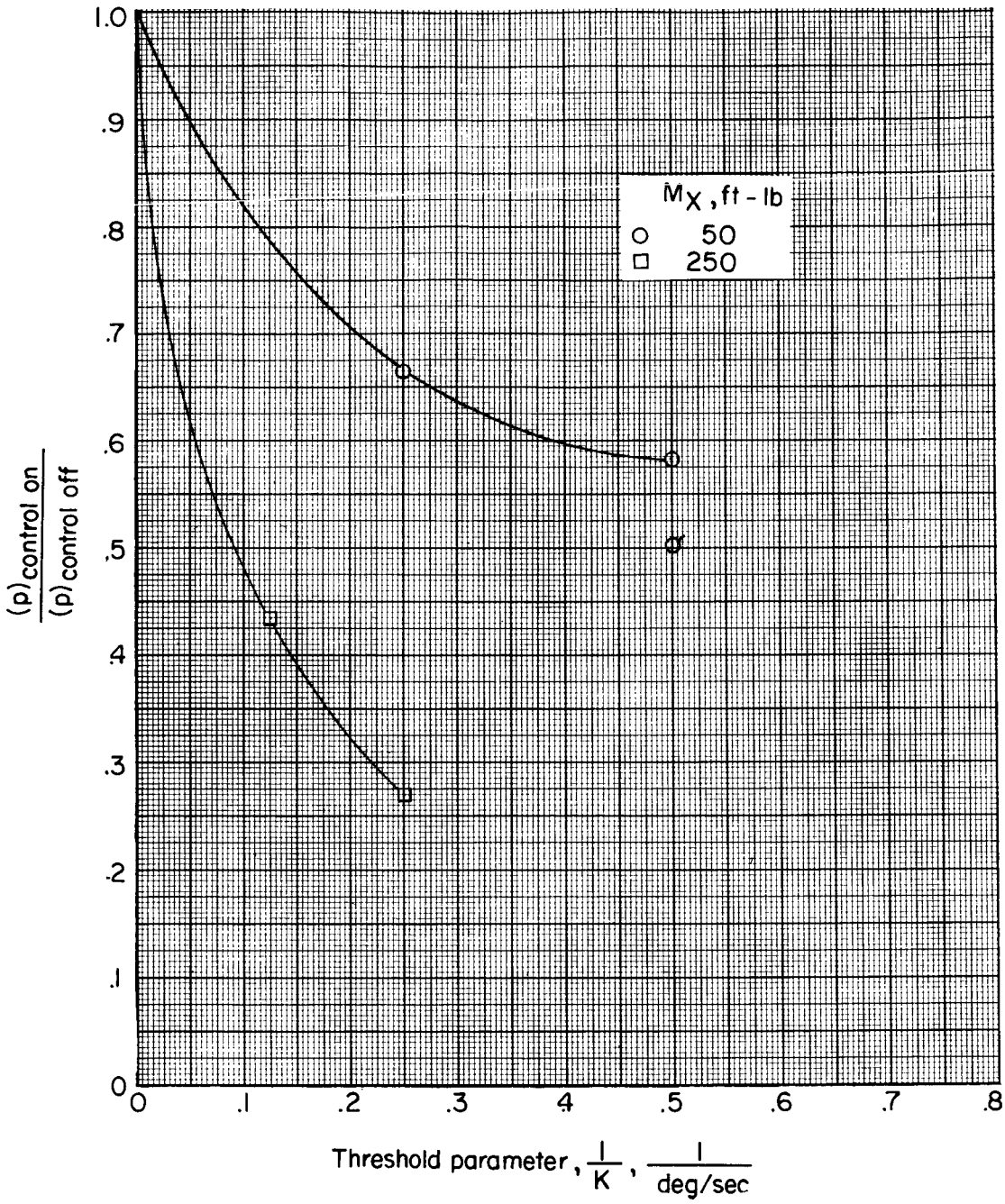

Figure 15.- Control effectiveness at an altitude of 160,000 feet. $\alpha_o = 10^o$; $p_o = 0^o$ per second; center-of-gravity offset, 4.9 percent d; $C_l' = 0.003$. Plain symbols, $\phi = 0^o$; flagged symbol, $\phi_o = 90^o$.

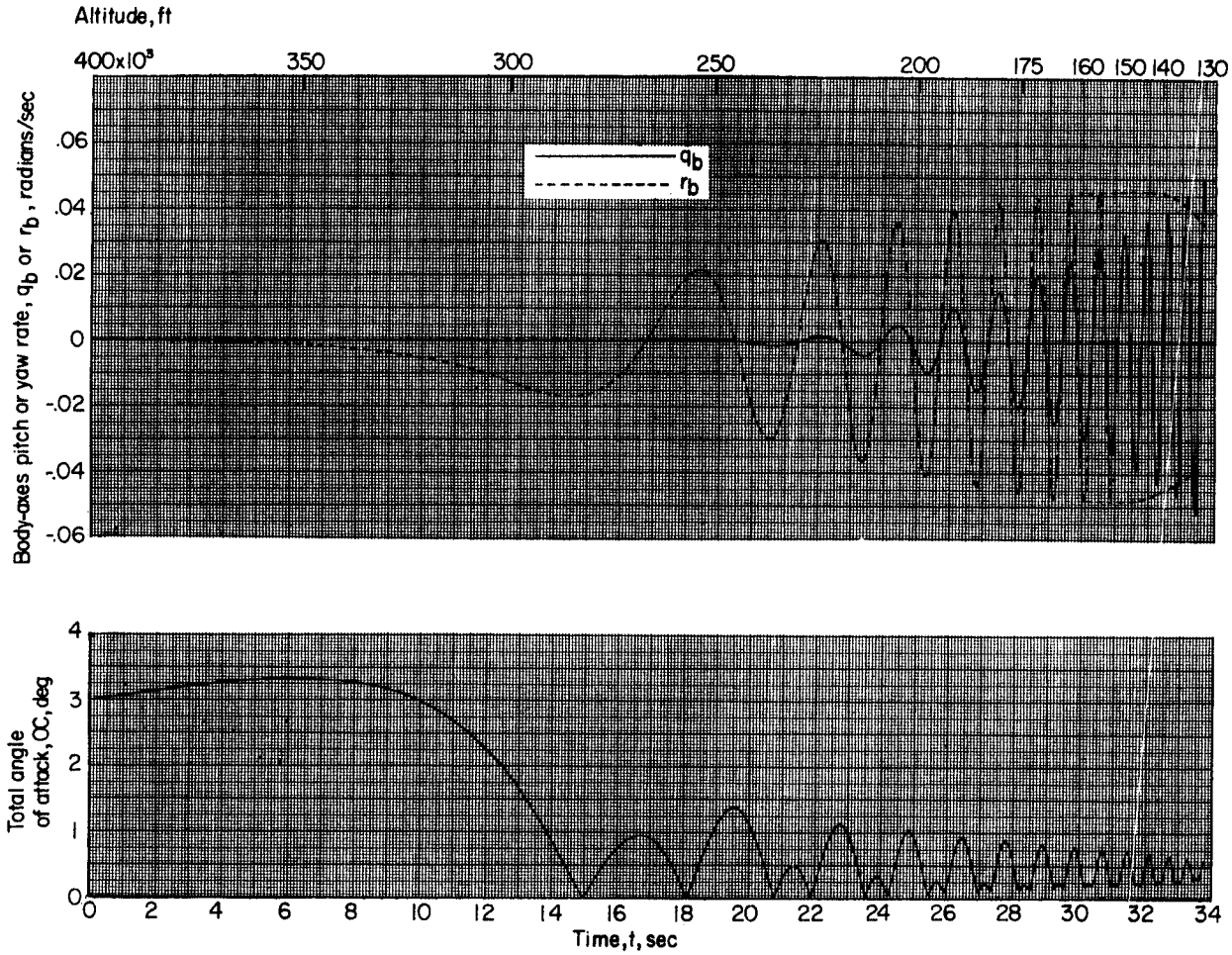

(a) Pitch rate, yaw rate, and angle-of-attack time histories.

Figure 16.- Reentry. $\alpha_o = 3^o$; $p_o = 0^o$ per second; $\phi_o = 90^o$; center-of-gravity offset, 2 percent d; $C_l' = 0.003$; $K = 5^o$ per second; $M_X = 250$ foot-pounds.

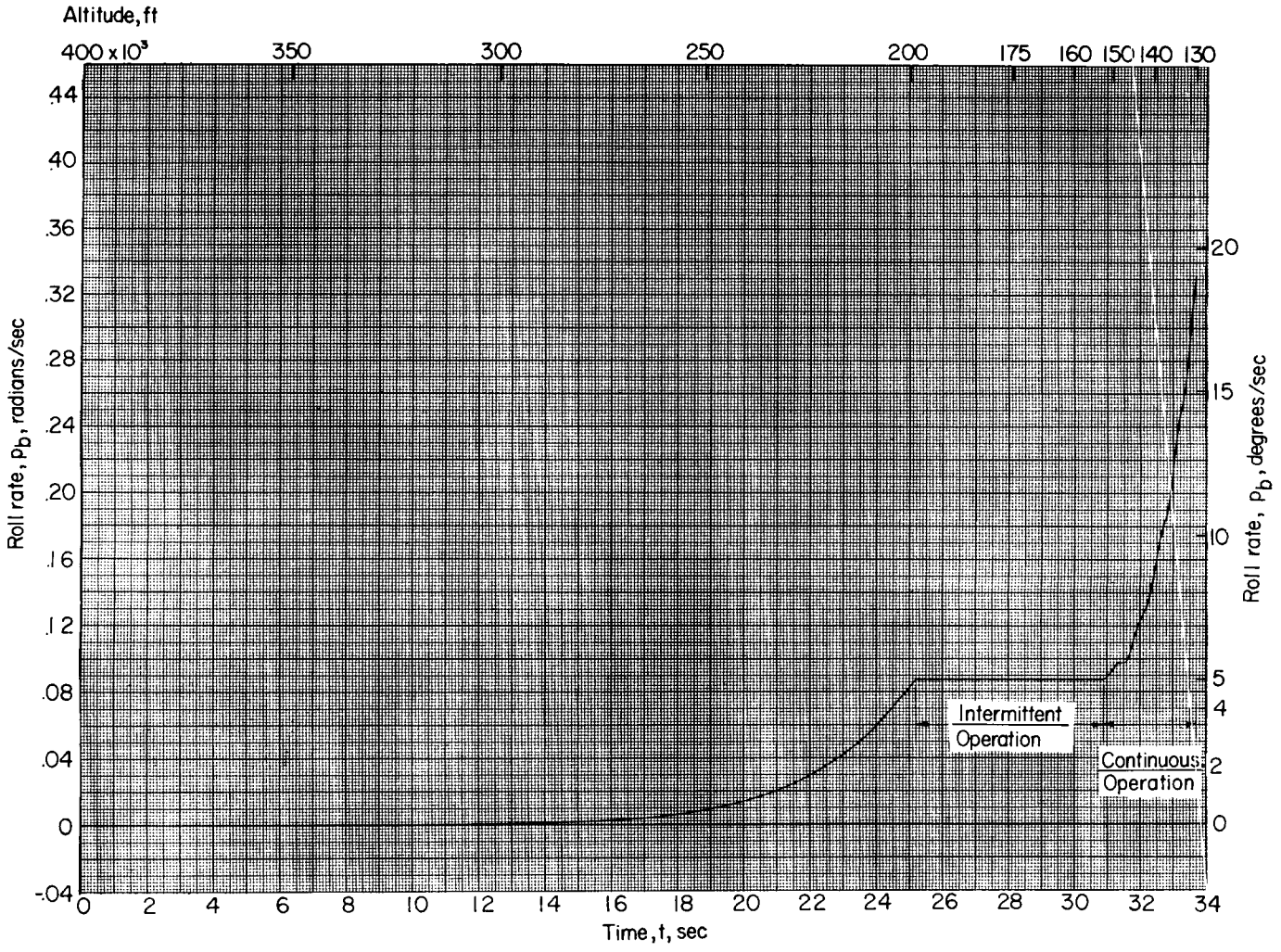

(b) Roll-rate time history.

Figure 16.- Continued.

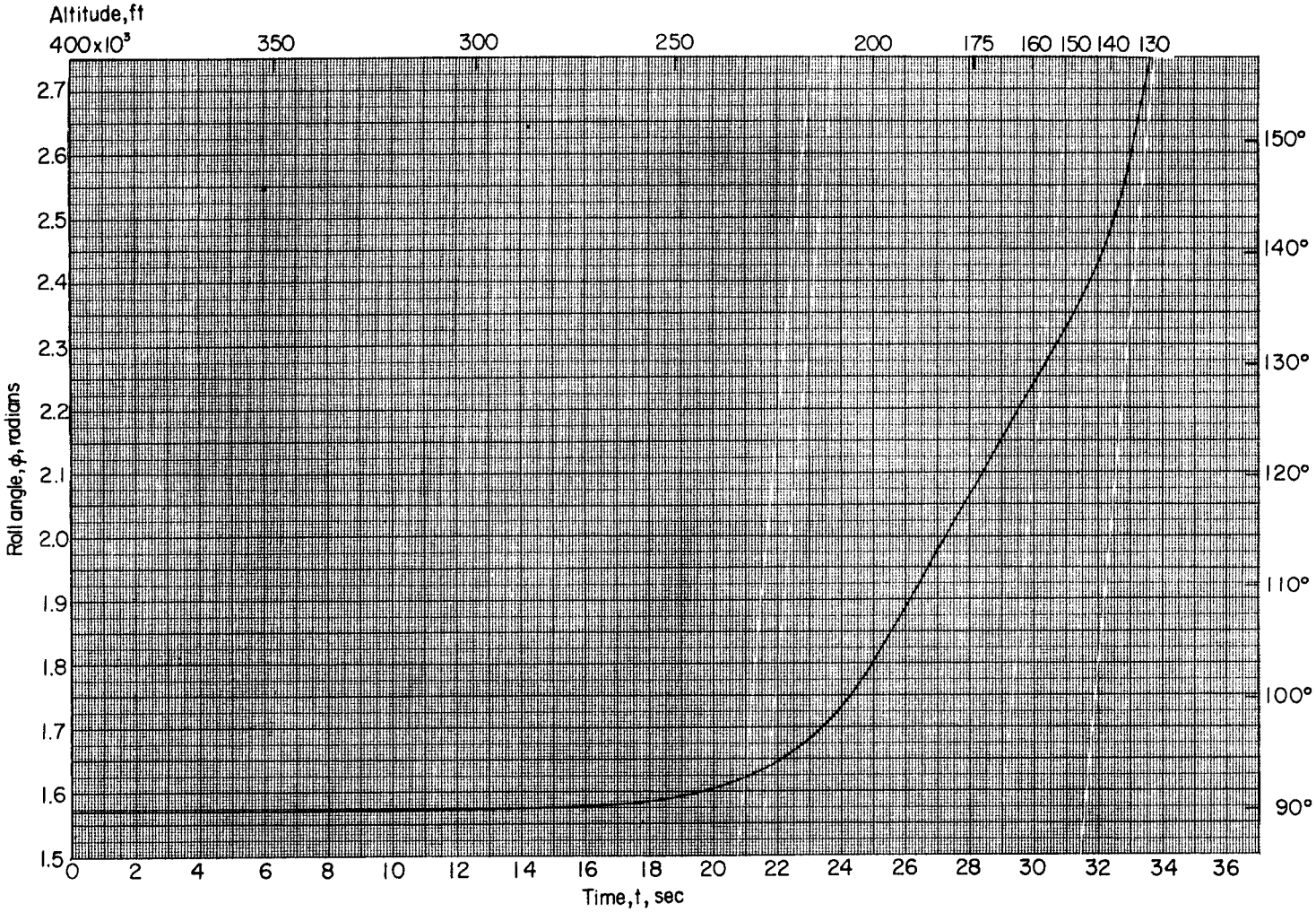

(c) Roll-angle time history.

Figure 16.- Continued.

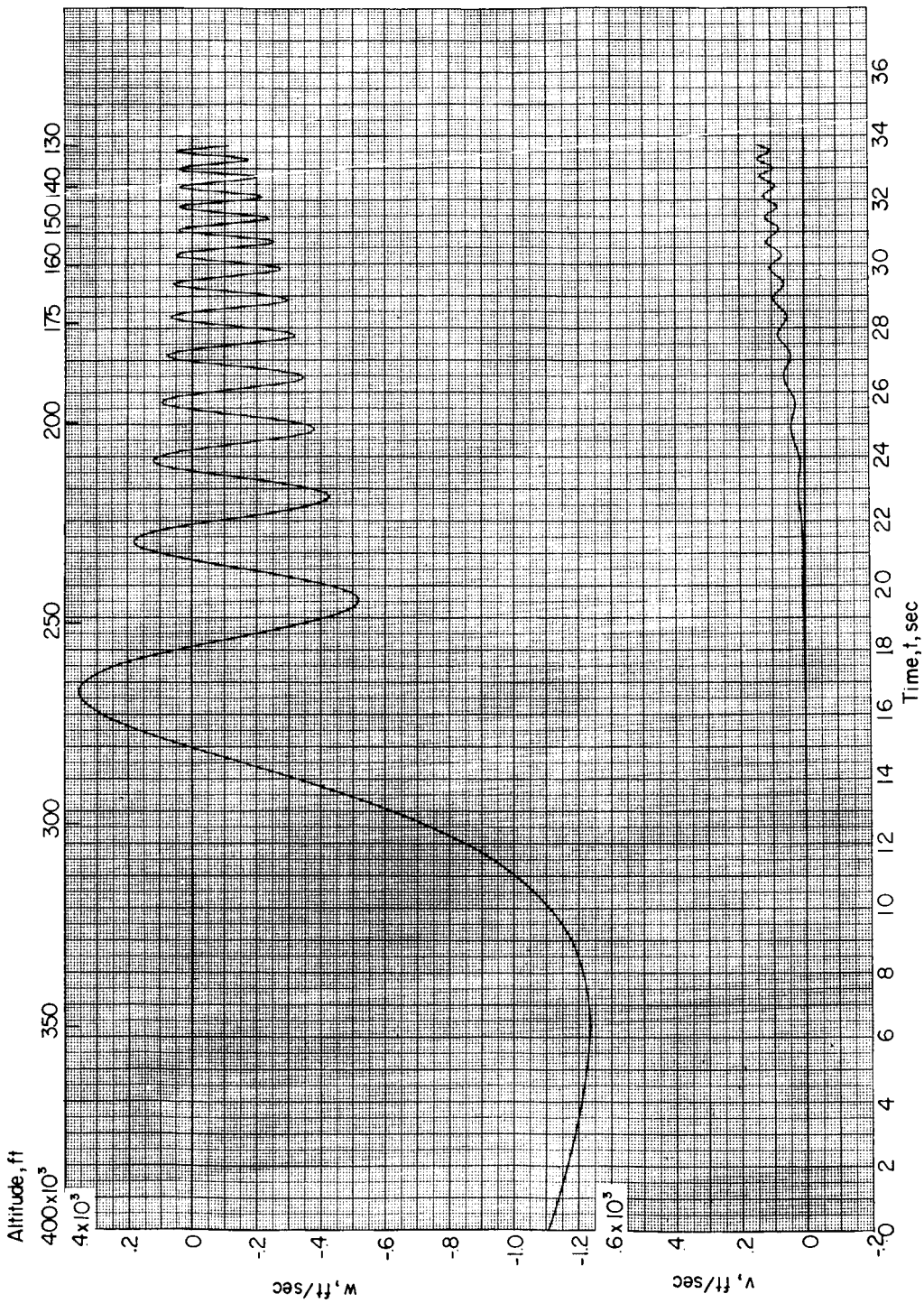

(d) w and v time histories.

Figure 16.- Concluded.

L-2058